

Sovereign Stress Avalanches and Network Amplification in Latin America

Diego Vallarino*

April 2026

Abstract

This paper studies sovereign stress avalanches and network amplification in Latin American credit markets using monthly J.P.M-EMBI Global Diversified spreads for eleven sovereigns, 2007–2026. Country stress events are defined as positive log-spread innovations exceeding country-specific volatility thresholds; regional avalanches count the number of stressed countries in each month. The empirical design combines finite-sample power-law diagnostics, threshold robustness, a country-level reshuffling placebo, and rolling correlation, partial-correlation, and minimum-spanning-tree networks. Avalanche sizes are heavy-tailed, with an estimated exponent of 1.77, while spread changes and inter-event times lie in a heavy-tail boundary regime. The placebo shows synchronization far above independent stress timing ($p < 0.001$). Large avalanches coincide with denser, more spectrally amplifying raw-correlation networks, but not after partial-correlation filtering, indicating common-factor comovement rather than conditional regional propagation. Network metrics describe contemporaneous stress regimes, not early-warning signals. The results provide a finite-size criticality framework for monitoring sovereign fragility in emerging markets.

Keywords: Self-organized criticality; sovereign spreads; EMBI; Latin America; financial networks; spectral fragility; contagion; finite-size criticality.

JEL codes: G15, F34, C58, E44, F65.

1 Introduction

The Latin American sovereign credit market exhibits empirical patterns that sit uncomfortably with standard macroeconomic intuition. Argentine spreads multiplied 2.5-fold in a single month after the August 2019 PASO primaries while Chilean spreads moved

*Inter-American Development Bank (IDB), Washington, DC, United States. Email: diegoval@iadb.org. The views expressed in this paper are strictly those of the author and do not necessarily represent the views of the Inter-American Development Bank, its Board of Directors, or the countries they represent.

within a 50 basis-point envelope; Ecuador defaulted twice within a decade with peak spreads above 5,000 basis points, yet Peru held below 300; in March 2020 every country in the region experienced a simultaneous large spread blowout. The combination of country-level idiosyncrasy and synchronized regional stress is anomalous and calls for analytical tools that capture both phenomena within a single framework.

The standard sovereign-spread literature explains spread levels through fiscal and external fundamentals (Edwards, 1984; Eichengreen and Mody, 1998; Longstaff et al., 2011; Hilscher and Nosbusch, 2010a) and treats contagion as a second-order correlation phenomenon (Forbes and Rigobon, 2002; Kaminsky and Reinhart, 2000; Kaminsky et al., 2003). The framework has been productive but has three limitations relevant to the present paper. First, it does not naturally explain the heavy-tailed distribution of spread changes (Mandelbrot, 1963; Gabaix, 2009). Second, it cannot identify whether observed synchronization reflects genuine network propagation or coincident reactions to common shocks; correlation-based diagnostics have been criticized for being driven by heteroscedasticity (Forbes and Rigobon, 2002). Third, it provides no operational measure of how close the system is to a regime transition.

A complementary tradition exists in econophysics. Self-organized criticality, introduced by Bak et al. (1987, 1988), describes systems that endogenously evolve toward critical states, producing power-law distributions of event sizes and inter-event times without external parameter tuning. The framework was introduced into economics by Bak et al. (1993) and Scheinkman and Woodford (1994a) and developed within the network tradition by Acemoglu et al. (2012), who showed that interconnected sectors can endogenously generate heavy-tail aggregate fluctuations from idiosyncratic shocks. Sandhu et al. (2016) demonstrated that Ricci curvature on financial networks tracks fragility prior to market downturns. Despite this conceptual maturity, the SOC framework has not been systematically applied to sovereign credit markets, and especially not to Latin America, where eighteen years of EMBI data covering the global financial crisis, the Eurozone shock, the taper tantrum, the COVID-19 rout, and the 2022–2025 Fed cycle furnish a natural laboratory.

This paper closes the gap. Five contributions follow. First, the paper conducts the first empirical SOC-style analysis of LATAM sovereign credit using monthly EMBI spreads for eleven countries over October 2007 to April 2026. Second, it documents that three independent statistical objects—avalanche size, absolute spread change, and inter-event times—all exhibit the heavy-tail boundary regime described by Stumpf and Porter (2012), in which power-law cannot be rejected against lognormal at conventional significance levels but thin-tailed alternatives are clearly inappropriate. Third, the paper reformulates the prediction of which countries are “critical”: not the high-spread fiscally stressed economies, but the mid-credibility highly traded ones. Fourth, the paper introduces a Spectral Fragility Index (SFI) on rolling co-movement networks as a

contemporaneous descriptor of regional fragility regimes. The SFI discriminates large-avalanche from non-large-avalanche windows in the raw correlation filter, although this regime difference is not robust to partial-correlation filtering, which suggests that most of the network amplification signal observed during stress episodes is driven by common-factor co-movement rather than by additional conditional regional propagation. Lead-lag predictive associations at the three-month horizon are not statistically significant in this sample, so the SFI is presented as a descriptive surveillance tool rather than as an early-warning instrument. Fifth, the paper implements a $B = 1,000$ country-level reshuffling placebo that formally distinguishes genuine multi-country synchronization from coincident independent stress. This is the strongest empirical result of the paper: observed regional synchronization is far larger than what is achievable under the independence null, with $p < 0.001$ across all four synchronization statistics.

The findings have implications beyond academic SOC. The fact that observed synchronization is dominated by intermediate-credibility, well-integrated sovereigns challenges the policy presumption that regional fragility is a “weak link” phenomenon driven by peripheral economies. It instead suggests that fragility in LATAM is an emergent property of capital-market integration itself: countries such as Brazil, Mexico, Peru, Colombia, and Panama participate repeatedly in regional stress episodes not because they are the most fiscally vulnerable, but because they are sufficiently liquid, investable, and embedded in global emerging-market portfolios to react to every meaningful shift in international risk appetite.

The paper is also disciplined about what it does not establish. The heavy-tail evidence is consistent with finite-size criticality but does not prove a unique asymptotic power law, since lognormal alternatives cannot be decisively rejected and the number of avalanche events is moderate ($n = 40$). The placebo test rules out independent country-level timing as the source of synchronization but does not separate endogenous regional propagation from exogenous common-factor responses. The network amplification result is contemporaneous rather than predictive. These boundaries are stated explicitly because the contribution of the paper is empirical discipline, not maximalist claims: LATAM sovereign credit markets display heavy-tailed, synchronized, threshold-robust stress avalanches whose largest events coincide with historically meaningful global episodes, and whose contemporaneous network environment becomes denser and more spectrally integrated, with the partial-correlation evidence suggesting that this integration is largely common-factor driven.

The remainder of the paper is organized as follows. Section 2 reviews the literature. Section 3 develops the theoretical framework and states six formal hypotheses. Section 4 describes the data and Section 5 the methodology. Section 6 reports the empirical results. Section 7 discusses implications and Section 8 concludes.

2 Literature Review

This paper lies at the intersection of four literatures: sovereign credit risk in emerging markets, financial contagion and connectedness, nonlinear dynamics and self-organized criticality, and network-based measures of systemic fragility. Its contribution is to bring these strands together in a setting where sovereign stress is observed not only as a sequence of country-specific spread movements, but as a finite-size regional propagation process.

The first strand is the empirical literature on sovereign spreads. The early benchmark is [Edwards \(1984\)](#), who established the link between sovereign borrowing costs, default risk, and macroeconomic fundamentals in developing countries. Subsequent work extended this framework to emerging-market bonds, showing that spreads reflect both domestic fundamentals and global financial conditions. [Eichengreen and Mody \(1998\)](#) document the joint role of country characteristics and market sentiment in emerging-market debt pricing, while [Hilscher and Nosbusch \(2010b\)](#) show that macroeconomic fundamentals, political risk, and external vulnerabilities jointly shape sovereign risk premia. [Longstaff et al. \(2011\)](#), using sovereign CDS data, find that global factors account for a large share of sovereign credit-risk variation, implying that sovereign spreads are not purely national objects but also reflect common financial conditions. This finding is especially relevant for Latin America, where the EMBI market is shaped by global risk appetite, benchmark rebalancing, and regional portfolio allocation.

A related literature emphasizes the historical recurrence of sovereign debt crises and the nonlinear nature of sovereign-risk regimes. [Reinhart and Rogoff \(2009\)](#) document long-run cycles of default, financial repression, and debt overhang, while [Reinhart and Trebesch \(2016\)](#) show that sovereign crises are embedded in global waves of capital flows, commodity prices, and international liquidity. Theoretical models of sovereign debt have also emphasized coordination and multiple equilibria. [Calvo \(1988\)](#) shows how self-fulfilling expectations can generate debt crises even when fundamentals do not uniquely determine the outcome, while [Cole and Kehoe \(2000\)](#) develop a model in which rollover crises arise from coordination failures among creditors. These contributions suggest that sovereign stress may involve threshold behavior and regime shifts, but they do not directly measure the cross-country synchronization of stress events. The present paper complements this literature by treating synchronized spread jumps as empirical avalanches and by studying their distribution and network environment.

The second strand is the literature on contagion, spillovers, and financial connectedness. [Forbes and Rigobon \(2002\)](#) provide the canonical critique of correlation-based contagion tests, showing that correlations mechanically rise during high-volatility periods and may therefore overstate contagion. This critique is central to the design of the present paper, which reports raw correlation networks but gives greater interpretive weight to partial-correlation and filtered network structures. [Kaminsky and Reinhart \(2000\)](#) and

Kaminsky et al. (2003) identify trade, financial integration, common lenders, and investor behavior as channels through which crises can spread across emerging markets. Bekaert et al. (2014b) and Bekaert et al. (2014a) further show that political and institutional shocks can generate cross-border asset-price responses that are not reducible to direct fundamental exposure. In the connectedness tradition, Diebold and Yilmaz (2014) introduce variance-decomposition-based measures of systemic connectedness, providing a framework for quantifying directional spillovers across financial markets. The present paper differs from this literature by focusing not on average spillover intensity, but on the size distribution of synchronized sovereign-stress events and on whether network amplification rises around large avalanches.

The third strand concerns the network origins of aggregate fluctuations and systemic risk. Acemoglu et al. (2012) show that idiosyncratic shocks can generate aggregate fluctuations when the production network is sufficiently asymmetric, thereby overturning the standard diversification logic. In a related financial setting, Acemoglu et al. (2015) show that interbank networks can be either shock absorbers or shock amplifiers depending on the size of shocks and the topology of the system. Haldane and May (2011) argue that financial complexity can increase systemic fragility when dense connectivity facilitates contagion rather than diversification. Glasserman and Young (2016) clarify the conditions under which financial networks amplify or dampen losses, emphasizing the role of leverage, concentration, and propagation structure. These papers motivate the spectral approach used here. In a linear propagation system, the spectral radius of the weighted adjacency matrix captures proximity to the stability boundary; as the spectral radius rises, the system becomes more capable of amplifying shocks. The Spectral Fragility Index used in this paper is a reduced-form operationalization of this idea in the context of sovereign-spread co-movement networks.

The fourth strand is the literature on nonlinear dynamics, heavy tails, and self-organized criticality. Mandelbrot (1963) first documented the empirical inadequacy of Gaussian models for speculative price changes. Bak et al. (1987) and Bak et al. (1988) introduced self-organized criticality as a mechanism through which locally interacting systems endogenously approach a critical state and generate power-law event-size distributions. Bak (1996) provides the canonical exposition of sandpile dynamics and avalanche distributions. In economics, Bak et al. (1993) and Scheinkman and Woodford (1994b) argue that sectoral interactions can generate aggregate fluctuations with critical properties, while Lux and Marchesi (1999) show that agent-based financial markets can produce scaling laws through endogenous interaction among heterogeneous traders. Gabaix et al. (2003) and Gabaix (2009) review the prevalence of power laws in economic and financial phenomena, and Sornette (2003) develops the concept of critical events and “dragon-kings” as extreme outcomes generated by endogenous amplification mechanisms.

The empirical challenge in this literature is that finite samples often do not allow clean

discrimination between power-law and lognormal alternatives. [Clauset et al. \(2009\)](#) provide the standard maximum-likelihood framework for estimating power-law tails and selecting the lower cutoff, while [Vuong \(1989\)](#) provides the non-nested likelihood-ratio logic used to compare power-law and lognormal specifications. [Stumpf and Porter \(2012\)](#) stress that many empirical claims about power laws are overstated because several heavy-tailed alternatives can fit the same data. This warning is directly relevant here. The present paper therefore avoids claiming that Latin American EMBI spreads obey a pure asymptotic power law. Instead, it tests whether avalanche sizes, absolute spread changes, and inter-event times lie in a heavy-tail boundary regime consistent with finite-size criticality. The object of interest is not the isolated distribution of $|\Delta s|$ alone, but the joint evidence of heavy-tailed avalanches, non-random synchronization, and network amplification.

A further methodological strand concerns filtered financial networks and geometric measures of fragility. [Mantegna \(1999\)](#) introduced the minimum spanning tree as a filtering device for extracting the hierarchical structure of financial correlations, and [Tuminello et al. \(2005\)](#) extended the logic of information filtering in financial networks. Ricci curvature has more recently been used to measure the fragility of networked financial systems. [Forman \(2003\)](#) introduced a combinatorial curvature for weighted cell complexes, while [Ollivier \(2009\)](#) developed a probabilistic notion of Ricci curvature based on optimal transport between neighborhood measures. [Sandhu et al. \(2016\)](#) apply Ricci curvature to financial networks and show that curvature-based measures can track market fragility prior to crises. In the present paper, curvature is treated as an auxiliary measure of geometric integration, while the main amplification results are based on density, node-strength concentration, spectral radius, and the Spectral Fragility Index. This distinction is important because sovereign-spread networks during global stress often become dense and geometrically integrated, so positive curvature may reflect redundant co-movement rather than bottleneck fragility.

The paper is also connected to recent work on nonlinear dynamic graphs in economic systems. [Vallarino \(2026c\)](#) studies stochastic network survival models in which propagation on economic graphs shapes time-to-event outcomes. [Vallarino \(2026a\)](#) examines identification and inference in nonlinear dynamic network models, emphasizing dependence, spectral structure, and empirical interpretation. [Vallarino \(2026b\)](#) develops a theoretical framework for sandpile economics, linking threshold accumulation, endogenous stress release, and heavy-tailed event distributions. The present paper complements this work by moving from theoretical and methodological formulations to an empirical sovereign-credit setting, where stress avalanches are measured directly from EMBI data and related to time-varying network amplification.

The gap addressed by this paper is therefore precise. Sovereign-spread models explain why countries become risky; contagion models explain why spreads co-move; network models explain how shocks propagate; and criticality models explain why event sizes may

be heavy-tailed. What is missing is an empirical framework that treats sovereign stress as a finite-size regional avalanche process and tests whether large synchronized events are statistically non-trivial and dynamically related to network amplification. This paper provides that framework for Latin American sovereign credit markets.

3 Theoretical Framework and Hypotheses

3.1 A finite-size sovereign-stress system

Consider a finite regional system of $n = 11$ Latin American sovereigns indexed by $c \in \{1, \dots, n\}$ and observed at monthly frequency. Let $s_{c,t} > 0$ denote the stripped EMBI Global Diversified spread of sovereign c at month t , and define the monthly log-spread innovation as

$$x_{c,t} \equiv \Delta \log s_{c,t} = \log s_{c,t} - \log s_{c,t-1}. \quad (1)$$

The empirical object of interest is not only the marginal distribution of $x_{c,t}$, but the cross-sectional synchronization of large positive realizations of $x_{c,t}$ across countries.

To motivate the empirical construction, suppose that each sovereign has an unobserved stress stock $z_{c,t}$ that evolves according to a threshold-based network propagation process:

$$z_{c,t+1} = (1 - \delta_c)z_{c,t} + \beta_c g_t + \gamma_c f_{c,t} + \sum_{j \neq c} a_{j,c,t} \mathbf{1}(z_{j,t} > z_j^*) + \varepsilon_{c,t+1}, \quad (2)$$

where g_t is a common global financial factor, $f_{c,t}$ denotes country-specific fiscal, political, or external vulnerability news, $a_{j,c,t}$ captures time-varying regional transmission from sovereign j to sovereign c , and $\delta_c \in (0, 1)$ governs stress dissipation. A stress event occurs when the latent stock crosses a sovereign-specific threshold z_c^* . The observed spread innovation $x_{c,t}$ is interpreted as a noisy market manifestation of changes in the latent stress stock.

The empirical stress indicator is therefore defined as a country-normalized positive tail event:

$$I_{c,t}(\sigma) = \mathbf{1}[x_{c,t} > \sigma \hat{\sigma}_c], \quad \hat{\sigma}_c = \text{sd}(x_{c,t}), \quad (3)$$

where $\sigma > 0$ is a multiplicative threshold and the baseline specification uses $\sigma = 1.5$. This definition identifies large positive spread innovations relative to each country's own historical volatility, rather than imposing a common basis-point threshold on sovereigns with very different spread levels and volatilities.

A sovereign-stress avalanche is the cross-sectional number of countries in stress in month t :

$$S_t(\sigma) = \sum_{c=1}^n I_{c,t}(\sigma). \quad (4)$$

The process $\{S_t(\sigma)\}$ is a finite-size regional stress-size process. Large values of S_t indicate synchronized sovereign stress, while small values correspond to isolated country-level stress events.

3.2 Finite-size criticality and avalanche predictions

In the canonical self-organized criticality framework, locally interacting systems endogenously approach a critical state in which small perturbations can generate events of very different sizes (Bak et al., 1987, 1988; Bak, 1996). For an infinite system, the central prediction is a power-law distribution of event sizes. In a finite empirical sovereign system, however, the support of S_t is mechanically bounded by $n = 11$. The appropriate empirical claim is therefore not that the system satisfies an asymptotic power law, but that it exhibits finite-size signatures consistent with critical propagation.

The main SOC-consistent empirical prediction is that avalanche sizes are heavy-tailed:

$$\Pr(S_t \geq s) \sim s^{-(\alpha-1)} \quad \text{for } s \geq s_{\min}, \quad (5)$$

with an exponent in a range compatible with finite-size critical behavior. The second prediction is that stress recurrence is irregular rather than Poisson-like, implying heavy-tailed inter-event times. Let $\tau_{c,k}$ denote the waiting time between consecutive stress events for country c . Then a critical propagation process should generate a dispersed distribution of $\tau_{c,k}$, reflecting clustered stress episodes separated by calm periods. The third prediction is that the underlying spread innovations also display heavy-tailed magnitudes, although $|\Delta s_{c,t}|$ is not the primary SOC object. Individual spread changes may be shaped by jumps, liquidity shocks, and heterogeneous volatility, whereas the avalanche-size distribution captures regional synchronization.

Following Clauset et al. (2009), power-law exponents are estimated by maximum likelihood with the lower cutoff selected by minimizing the Kolmogorov–Smirnov distance. Following Vuong (1989), power-law fits are compared with lognormal alternatives through non-nested likelihood-ratio tests. The interpretation follows Stumpf and Porter (2012): in finite samples, failure to reject the lognormal alternative does not invalidate the heavy-tail claim. Rather, the relevant question is whether the data lie in a heavy-tail boundary regime in which Gaussian or exponential alternatives are clearly inappropriate and the power-law/lognormal distinction is empirically non-degenerate.

3.3 Dynamic network amplification

The latent propagation process in equation (2) implies that stress transmission depends on the time-varying network structure $A_t = [a_{ij,t}]$. Empirically, the network is not directly observed. I therefore approximate the sovereign-stress transmission structure using rolling

co-movement networks of EMBI spread innovations.

For each 24-month rolling window, three filtered networks are constructed on the common set of sovereigns $V = \{1, \dots, n\}$. The first is a correlation network, where an undirected edge is included when $|\rho_{ij,t}| > \rho^*$, with $\rho^* = 0.4$. The second is a partial-correlation network. Let Σ_t denote the covariance matrix of spread innovations in the rolling window and let $\Omega_t = \Sigma_t^{-1}$ denote the corresponding precision matrix. The partial correlation between sovereigns i and j is

$$\rho_{ij,t}^{\text{part}} = -\frac{\Omega_{ij,t}}{\sqrt{\Omega_{ii,t}\Omega_{jj,t}}}, \quad (6)$$

and an edge is included when $|\rho_{ij,t}^{\text{part}}| > \rho^*$. The third network is the minimum spanning tree computed from correlation distances $d_{ij,t} = 1 - |\rho_{ij,t}|$. The correlation network captures total co-movement, the partial-correlation network filters common linear dependence, and the minimum spanning tree provides a sparse topology with a fixed number of edges.

For each network, let $W_t = [w_{ij,t}]$ denote the weighted adjacency matrix. The first dynamic amplification measure is the normalized spectral radius:

$$\rho_t^\infty = \lambda_{\max} \left(\frac{W_t}{\|W_t\|_\infty} \right), \quad \rho_t^F = \lambda_{\max} \left(\frac{W_t}{\|W_t\|_F} \right), \quad (7)$$

where $\|W_t\|_\infty$ is the maximum row-sum norm and $\|W_t\|_F$ is the Frobenius norm. These normalizations avoid the mechanical unit eigenvalue that would arise from row-stochastic normalization. The Spectral Fragility Index is defined as

$$\text{SFI}_t = \frac{\rho_t}{1 - \rho_t}, \quad (8)$$

where ρ_t denotes either normalized spectral radius. In a linear propagation system of the form

$$y_t = W_t y_{t-1} + \eta_t, \quad (9)$$

the cumulative response to shocks is governed by the Neumann series $(I - W_t)^{-1}$, which becomes more amplifying as the spectral radius approaches the stability boundary. The SFI is therefore interpreted as a reduced-form indicator of the network's proximity to high-amplification propagation.

3.4 Network geometry

In addition to spectral amplification, I compute geometric summaries of the sovereign-spread network. The Forman–Ricci curvature of edge (u, v) is defined as

$$\kappa_{uv}^F = w_{uv} \left[\frac{w_u + w_v}{w_{uv}} - \sum_{\substack{e_u \sim u \\ e_u \neq uv}} \frac{w_{uv}}{\sqrt{w_{uv}w_{e_u}}} - \sum_{\substack{e_v \sim v \\ e_v \neq uv}} \frac{w_{uv}}{\sqrt{w_{uv}w_{e_v}}} \right], \quad (10)$$

following Forman (2003), where $w_u = \sum_{k \sim u} w_{uk}$ is node strength. I also compute a normalized Ollivier-style curvature based on optimal transport between neighborhood measures. The canonical Ollivier–Ricci curvature on edge (u, v) is

$$\kappa_{uv}^O = 1 - \frac{W_1(\mu_u, \mu_v)}{d(u, v)}, \quad (11)$$

where W_1 is the 1-Wasserstein distance between the probability measures induced on the neighborhoods of u and v (Ollivier, 2009). In the empirical implementation, distances are normalized to avoid spurious curvature explosions in highly correlated networks. Curvature is therefore interpreted as an auxiliary measure of geometric integration rather than as the primary measure of fragility. The main fragility indicators are spectral radius, SFI, density, and node-strength concentration.

3.5 Hypotheses

The theoretical framework implies six testable hypotheses. They are stated in terms of empirical objects that are directly measured in the data and tested in Section 6.

- H1. Avalanche-size heavy tails.** The distribution of sovereign-stress avalanche sizes is heavy-tailed and lies in a finite-size criticality regime. Operationally, the estimated tail exponent for $S_t(\sigma)$ should lie in a plausible critical range, and power-law behavior should not be decisively rejected in favor of lognormal alternatives.
- H2. Non-random synchronization.** Large sovereign-stress avalanches are not mechanically generated by country-specific stress frequencies. Operationally, a reshuffling placebo that preserves each country’s number of stress events but randomizes their timing should generate substantially smaller maximum avalanche sizes and lower shares of large avalanches than the observed data.
- H3. Threshold robustness.** The avalanche result should not be an artifact of the base-line threshold. Operationally, the estimated tail exponent and maximum avalanche size should remain within a stable range for stress thresholds between $\sigma = 1.25$ and $\sigma = 2.00$, with additional diagnostics reported up to $\sigma = 2.50$.

- H4. Heterogeneous country participation.** Country participation in stress avalanches is heterogeneous. Operationally, stress-event counts should reject uniform participation across countries, and the ranking of participation should not be mechanically ordered by average spread level.
- H5. Network amplification during large avalanches.** Large avalanche months are associated with more amplifying network states. Operationally, rolling network windows overlapping large stress episodes should display higher density, higher normalized spectral radius, higher SFI, or lower concentration than non-stress windows.
- H6. Predictive network association.** We test whether network amplification contains lead-lag predictive content for near-future regional stress. Operationally, we examine whether current network metrics in any of the three filters are associated with the maximum avalanche size observed over the subsequent three months. A finding of no significant association would indicate that the network metrics constructed here are descriptors of contemporaneous stress regimes rather than predictive instruments at the three-month horizon.

4 Data

The empirical analysis uses monthly J.P. Morgan EMBI Global Diversified stripped spreads for eleven Latin American sovereigns: Argentina (ARG), Brazil (BRA), Chile (CHL), Colombia (COL), Dominican Republic (DOM), Ecuador (ECU), Mexico (MEX), Panama (PAN), Peru (PER), El Salvador (SLV), and Uruguay (URY). The sample runs from October 2007 to April 2026, yielding a balanced monthly panel of 223 observations per country and 2,453 country-month observations in total. Spreads are expressed in basis points and are used as market-based measures of sovereign credit risk. The use of stripped spreads focuses the analysis on the sovereign credit-risk component embedded in EMBI bond prices, abstracting from collateralized components and other mechanical features of the underlying instruments.

The country coverage is chosen to maximize cross-sectional consistency within Latin America while preserving a long monthly time dimension. The resulting panel covers a heterogeneous set of sovereigns. Argentina, Ecuador, and El Salvador display substantially higher average spreads and larger right tails, whereas Chile, Peru, Uruguay, Panama, Brazil, Colombia, and Mexico trade at lower average spreads over most of the sample. This heterogeneity is useful for the purposes of the paper because it allows the empirical analysis to distinguish between two different notions of fragility: high average sovereign risk and frequent participation in synchronized regional stress episodes.

Table 1 reports the country-level coverage and descriptive statistics. All eleven series are observed without gaps over the same sample window. Argentina and Ecuador exhibit

the largest maximum spreads, with peaks of 3,803 and 5,129 basis points respectively, both associated with their 2020 sovereign credit events. Chile is the most stable sovereign in the panel, ranging between 87 and 392 basis points. These differences in levels and tail dispersion motivate the country-normalized event definition used in the next section: stress is measured relative to each sovereign’s own historical spread-change volatility rather than through a common basis-point threshold.

Table 1: Coverage and descriptive statistics of monthly EMBI Global Diversified stripped spreads, by country (basis points).

Code	Country	Start	End	N	Mean	Median	SD	Min	Max
ARG	Argentina	2007-10	2026-04	223	1,094	817	669	312	3,803
BRA	Brazil	2007-10	2026-04	223	260	241	75	140	548
CHL	Chile	2007-10	2026-04	223	156	144	47	87	392
COL	Colombia	2007-10	2026-04	223	248	223	89	112	575
ECU	Ecuador	2007-10	2026-04	223	1,077	824	775	361	5,129
MEX	Mexico	2007-10	2026-04	223	282	271	94	121	656
PAN	Panama	2007-10	2026-04	223	203	187	70	102	582
PER	Peru	2007-10	2026-04	223	182	168	60	107	530
DOM	Dom. Rep.	2007-10	2026-04	223	403	362	210	164	1,705
URY	Uruguay	2007-10	2026-04	223	198	181	111	64	834
SLV	El Salvador	2007-10	2026-04	223	610	459	430	158	2,704

Source: J.P. Morgan EMBI Global Diversified (monthly stripped spreads).

All series cover 2007:M10 to 2026:M4 ($N = 223$ months) without gaps.

Spreads in basis points. ARG and ECU exhibit extreme right tails reflecting the 2020 sovereign credit events.

The sample contains several major episodes of global and regional financial stress: the global financial crisis and post-Lehman emerging-market repricing (2008–2009), the European sovereign crisis and associated global risk-off episodes (2010–2012), the taper tantrum and emerging-market repricing (2013–2014), the commodity-price downturn and emerging-market sell-off (2015–2016), the Argentina currency and sovereign-risk crisis (2018–2019), the COVID-19 global financial shock (2020), and the Federal Reserve tightening cycle and post-pandemic repricing of emerging-market risk (2022–2025). The sample therefore spans both global common shocks and country-specific sovereign events, which is essential for separating ordinary co-movement from synchronized regional stress.

Figure 1 displays the eleven EMBI spread series on a logarithmic scale. Vertical red lines mark months in which at least six countries simultaneously exceed their country-specific stress thresholds. The figure highlights the empirical object studied in the paper: large regional stress months are not defined by the level of any single sovereign spread, but by the cross-sectional synchronization of large positive spread changes across the region. This distinction is central to the avalanche approach developed below.

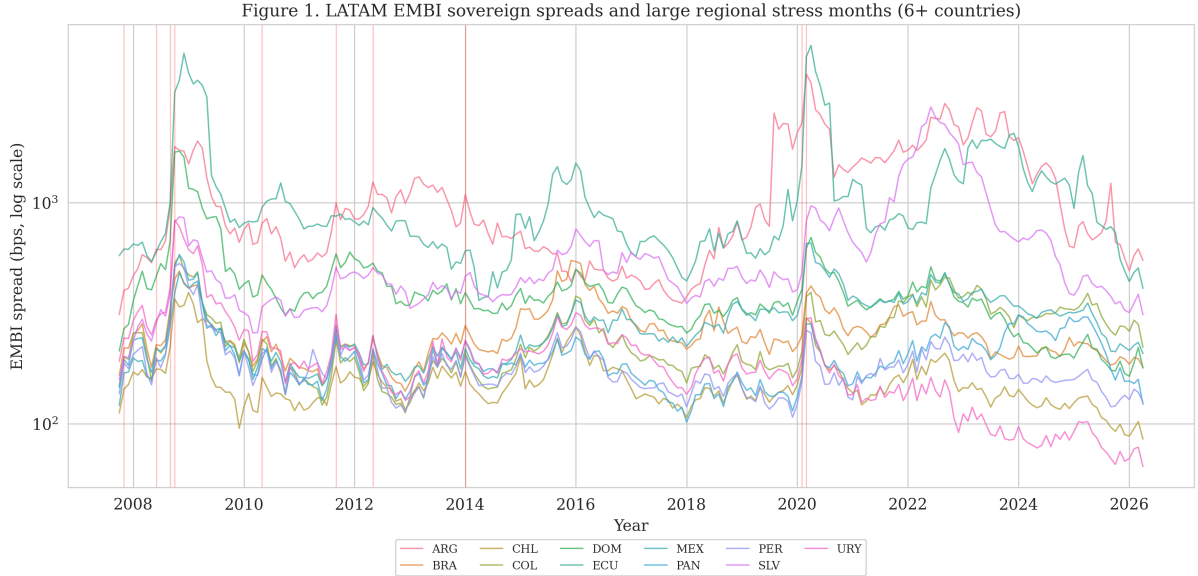


Figure 1: LATAM EMBI Global Diversified stripped sovereign spreads, 2007:M10–2026:M4. Spreads are monthly observations in basis points and are shown on a logarithmic scale. Vertical red lines identify large regional stress months, defined as months in which at least six sovereigns simultaneously exceed their country-specific stress threshold ($S_t \geq 6$).

The empirical analysis uses the spread panel in three ways. First, monthly log-spread changes are used to define country-level stress events. Second, the number of simultaneous stress events in each month defines the sovereign-stress avalanche size. Third, rolling windows of spread changes are used to construct time-varying co-movement networks. The same underlying EMBI panel therefore supports the three empirical layers of the paper: tail diagnostics, synchronization tests, and network-amplification analysis.

5 Methodology

This section describes the empirical procedure used to identify sovereign-stress avalanches, estimate tail behavior, construct filtered spread networks, and evaluate whether observed synchronization exceeds what would be expected under country-level stress frequencies alone. All tables are stored in the `tables/` folder and all figures in the `figures/` folder.

5.1 Avalanche identification

Let $s_{c,t}$ denote the EMBI stripped spread of sovereign c in month t , measured in basis points. I define the monthly log-spread innovation as

$$x_{c,t} = \Delta \log s_{c,t} = \log s_{c,t} - \log s_{c,t-1}. \quad (12)$$

For each country, I compute the full-sample standard deviation $\hat{\sigma}_c = \text{sd}(x_{c,t})$. A country-level stress event is identified when the positive log-spread innovation exceeds a country-

specific volatility threshold:

$$I_{c,t}(\sigma) = \mathbf{1} [x_{c,t} > \sigma \hat{\sigma}_c]. \quad (13)$$

The baseline specification uses $\sigma = 1.5$. Robustness exercises repeat the analysis for

$$\sigma \in \{1.25, 1.50, 1.75, 2.00, 2.25, 2.50\}.$$

This country-normalized threshold avoids imposing a common basis-point definition of stress on sovereigns with very different spread levels and volatility regimes.

The sovereign-stress avalanche size in month t is defined as the number of countries simultaneously in stress:

$$S_t(\sigma) = \sum_{c=1}^n I_{c,t}(\sigma). \quad (14)$$

Thus, $S_t = 1$ corresponds to an isolated country-level stress event, while large values of S_t indicate synchronized regional stress. In the empirical application, $n = 11$, so avalanche sizes are mechanically bounded between zero and eleven. This finite support is important for interpretation: the analysis tests for finite-size criticality signatures rather than for an asymptotic infinite-system power law.

5.2 Power-law estimation and tail diagnostics

The paper studies three related statistical objects: avalanche sizes S_t , absolute monthly spread changes $|\Delta s_{c,t}|$, and inter-event times $\tau_{c,k}$ between consecutive stress events for country c . For each object, I estimate the power-law exponent $\hat{\alpha}$ and lower cutoff x_{\min} using the maximum-likelihood procedure of [Clauset et al. \(2009\)](#). The cutoff x_{\min} is chosen by minimizing the Kolmogorov–Smirnov distance between the empirical and fitted complementary cumulative distribution functions.

The fitted power law is then compared with lognormal alternatives using the non-nested likelihood-ratio framework of [Vuong \(1989\)](#). I report the normalized log-likelihood ratio $R_{\text{PL/LN}}$ and its associated p -value. Positive values of $R_{\text{PL/LN}}$ favor the power law, while negative values favor the lognormal. Following [Stumpf and Porter \(2012\)](#), I do not interpret the analysis as a mechanical test of a pure asymptotic power law. Instead, the relevant question is whether the empirical distributions belong to a heavy-tail boundary regime in which Gaussian or exponential benchmark models are inappropriate and the power-law and lognormal specifications are difficult to separate decisively in finite samples.

The main object for the SOC interpretation is the avalanche-size distribution, not the marginal distribution of individual spread changes. Individual monthly spread changes may be influenced by liquidity shocks, rating news, country-specific jumps, and global risk appetite. Avalanche sizes instead measure the cross-sectional synchronization of stress

events, which is the relevant object for detecting regional propagation.

5.3 Filtered sovereign-spread networks

To study network amplification, I construct rolling networks of sovereign spread co-movement using 24-month windows of $x_{c,t} = \Delta \log s_{c,t}$. For each window ending in month t , three network filters are computed over the common set of eleven countries.

The first network is the absolute-correlation network, G_t^ρ . An undirected edge (i, j) is included when

$$|\hat{\rho}_{ij,t}| > \rho^*, \quad \rho^* = 0.4, \quad (15)$$

where $\hat{\rho}_{ij,t}$ is the sample correlation between spread innovations of sovereigns i and j within the rolling window. Edge weights are given by $w_{ij,t} = |\hat{\rho}_{ij,t}|$.

The second network is the partial-correlation network, G_t^{part} . Let Σ_t denote the covariance matrix of spread innovations in the rolling window and let $\Omega_t = \Sigma_t^{-1}$ denote the corresponding precision matrix. The partial correlation between sovereigns i and j is defined as

$$\hat{\rho}_{ij,t}^{\text{part}} = -\frac{\Omega_{ij,t}}{\sqrt{\Omega_{ii,t}\Omega_{jj,t}}}. \quad (16)$$

An edge is included when $|\hat{\rho}_{ij,t}^{\text{part}}| > \rho^*$, with weight $|\hat{\rho}_{ij,t}^{\text{part}}|$. This network is intended to reduce the influence of common linear dependence and to isolate conditional co-movement among sovereigns.

The third network is the minimum spanning tree, G_t^{MST} , computed from correlation distances

$$d_{ij,t} = 1 - |\hat{\rho}_{ij,t}|. \quad (17)$$

Following the filtering logic of Mantegna (1999) and Tumminello et al. (2005), the MST preserves the strongest hierarchical co-movement structure while imposing a fixed number of edges. Since the system contains $n = 11$ sovereigns, each MST contains exactly $n - 1 = 10$ edges.

The correlation network captures total co-movement, the partial-correlation network captures conditional co-movement, and the MST provides a sparse topological benchmark. The comparison across these three filters is important because raw correlations may become mechanically dense during high-volatility episodes, whereas filtered networks provide a more conservative view of regional stress transmission.

5.4 Network amplification and geometry

For each network snapshot, I compute density, the Herfindahl–Hirschman index of node strengths, spectral amplification measures, and curvature-based geometric summaries. Let $W_t = [w_{ij,t}]$ denote the weighted adjacency matrix of a given network at time t .

Network density is the realized share of possible undirected edges, while the HHI of node strengths is defined as

$$HHI_t = \sum_{c=1}^n \left(\frac{\sum_j w_{cj,t}}{\sum_i \sum_j w_{ij,t}} \right)^2. \quad (18)$$

A lower HHI indicates that network strength is more evenly distributed across sovereigns.

The main amplification measures are normalized spectral radii. I use two normalizations:

$$\rho_t^\infty = \lambda_{\max} \left(\frac{W_t}{\|W_t\|_\infty} \right), \quad \rho_t^F = \lambda_{\max} \left(\frac{W_t}{\|W_t\|_F} \right), \quad (19)$$

where $\|W_t\|_\infty$ is the maximum row-sum norm and $\|W_t\|_F$ is the Frobenius norm. These normalizations avoid the mechanical unit eigenvalue that would arise from row-stochastic normalization. The Spectral Fragility Index is defined as

$$SFI_t = \frac{\rho_t}{1 - \rho_t}, \quad (20)$$

where ρ_t denotes either normalized spectral radius. The index increases nonlinearly as the network approaches the high-amplification boundary $\rho_t \rightarrow 1$.

I also compute Forman–Ricci and Ollivier–Ricci curvature measures. Mean Forman–Ricci curvature, $\bar{\kappa}_t^F$, is computed using Equation (10). Mean Ollivier–Ricci curvature, $\bar{\kappa}_t^O$, is computed through an optimal-transport problem between neighborhood measures, as in Equation (11). In the empirical interpretation, curvature is treated as an auxiliary measure of geometric integration. The primary fragility indicators are the spectral radius, SFI, density, and HHI, because these quantities map more directly into amplification and synchronization.

5.5 Placebo synchronization test

A key concern is that large avalanches may arise mechanically from country-level stress frequencies. To address this concern, I implement a country-level reshuffling placebo. For each replication $b = 1, \dots, B$, with $B = 1,000$, the stress indicator sequence $I_{c,t}(\sigma)$ is independently shuffled across calendar months within each country. This procedure preserves the number of stress events for each sovereign, but destroys cross-country timing.

For each placebo replication, I recompute the avalanche-size process $S_t^{(b)}$ and four synchronization statistics:

$$\max_t S_t^{(b)}, \quad \mathbb{E}[S_t^{(b)} \mid S_t^{(b)} > 0], \quad \Pr(S_t^{(b)} \geq 4), \quad \Pr(S_t^{(b)} \geq 6).$$

The placebo p -value is the share of replications in which the placebo statistic equals or exceeds its observed counterpart. This test directly asks whether the observed regional synchronization is stronger than what would be expected from independent country-level

stress timing.

5.6 Lead-lag network association

Finally, I evaluate whether network amplification contains early-warning information about subsequent regional stress. For each network metric m_t computed at snapshot t , I define the future three-month avalanche outcome as

$$Y_t = \max_{u \in (t, t+3]} S_u. \quad (21)$$

I then compute Pearson correlations and simple heteroskedasticity-robust OLS associations between m_t and Y_t . These regressions are not interpreted as causal estimates. Their purpose is to assess whether contemporaneous network states are informative about near-future regional stress intensity. The main metrics of interest are the spectral radius, SFI, network density, and HHI, especially in the partial-correlation network.

6 Empirical Results

This section reports the empirical evidence in six steps, following the order of hypotheses stated in Section 3. I first evaluate whether sovereign-stress avalanche sizes exhibit heavy-tailed behavior (H1). I then test whether the observed synchronization is stronger than what would be expected from country-level stress frequencies alone (H2). I next examine threshold robustness (H3), country participation heterogeneity (H4), network amplification during large avalanche regimes (H5), and the lead-lag association between network states and subsequent regional stress (H6).

6.1 Avalanche-size heavy tails (H1)

Table 2 reports formal tail diagnostics for three statistical objects: avalanche sizes S_t , absolute monthly EMBI spread changes $|\Delta_{S_c,t}|$, and inter-event times $\tau_{c,k}$ between consecutive stress events of country c . The baseline avalanche-size distribution yields an estimated exponent of $\hat{\alpha} = 1.77$ with $x_{\min} = 1$. The likelihood-ratio comparison against the lognormal alternative is negative, $R_{PL/LN} = -1.61$, but not statistically decisive at conventional levels ($p_{LN} = 0.107$). The evidence does not uniquely identify a pure power law, but it is consistent with a finite-size heavy-tailed avalanche distribution. The number of avalanche events above the estimated cutoff ($n = 40$) is below the threshold of $n \geq 50$ that [Clauset et al. \(2009\)](#) recommend for stable maximum-likelihood estimation, which provides an additional reason to interpret the exponent estimate cautiously.

Pooled absolute monthly spread changes also display heavy-tailed behavior, with $\hat{\alpha} = 2.37$ and $x_{\min} \simeq 86$ basis points. The comparison against the lognormal is again not

decisive ($R_{\text{PL/LN}} = -0.76$, $p_{\text{LN}} = 0.448$), although the exponential alternative is strongly rejected ($R_{\text{PL/Exp}} = 3.43$, $p = 0.001$). Inter-event times produce a similar conclusion, with $\hat{\alpha} = 2.38$, $x_{\min} = 12$ months, and no decisive likelihood-ratio separation from the lognormal. Taken together, the results place the EMBI system in the heavy-tail boundary regime emphasized by [Stumpf and Porter \(2012\)](#): the relevant empirical claim is not that a pure asymptotic power law is proven, but that avalanche sizes, spread changes, and waiting times are all far from thin-tailed benchmark behavior.

Panel A. Power-law tail estimates

Table 2: Tail diagnostics for SOC-relevant statistical objects in LATAM EMBI data

Object	n	x_{\min}	$\hat{\alpha}$	KS D
Avalanche size S_t	40	1.000	1.771	0.095
$ \Delta s_{c,t} $ pooled	2442	85.459	2.372	0.028
Inter-event times (months)	129	11.991	2.381	0.084

Panel B. Likelihood-ratio comparisons and interpretation

Object	$R_{\text{PL/LN}}$	p_{LN}	$R_{\text{PL/Exp}}$	p_{Exp}	Verdict
Avalanche size S_t	-1.612	0.107	-0.502	0.616	Heavy-tail boundary; PL not decisively rejected vs. LN
$ \Delta s_{c,t} $ pooled	-0.758	0.448	3.426	0.001	Heavy-tail boundary; PL favored over Exp
Inter-event times (months)	-0.606	0.544	1.106	0.269	Heavy-tail boundary; PL not decisively rejected vs. LN

$\hat{\alpha}$ and x_{\min} are maximum-likelihood estimates of the power-law tail exponent and lower cutoff, respectively, following [Clauset et al. \(2009\)](#). KS D is the Kolmogorov–Smirnov distance from the fitted power law above x_{\min} .

$R_{\text{PL/LN}}$ and $R_{\text{PL/Exp}}$ are Vuong normalized log-likelihood ratios comparing the power-law model against lognormal and exponential alternatives, respectively. Positive values favor the power-law model.

The results support a conservative heavy-tail boundary interpretation in the sense of [Stumpf and Porter \(2012\)](#): power-law and lognormal alternatives are difficult to discriminate in finite samples, while the exponential benchmark is clearly rejected only for pooled absolute spread changes.

The avalanche-size evidence should therefore be interpreted as finite-size criticality evidence, not as proof of a unique asymptotic power law.

Figure 2 displays the empirical avalanche-size CCDF and the country participation ranking. Panel A shows that most stress events are small, but the upper tail includes regional avalanches involving a large share of the system. Panel B shows that participation is highly heterogeneous across sovereigns, a result analyzed further in Section 6.4.

Figure 2. Empirical sovereign-stress avalanches in LATAM EMBI spreads

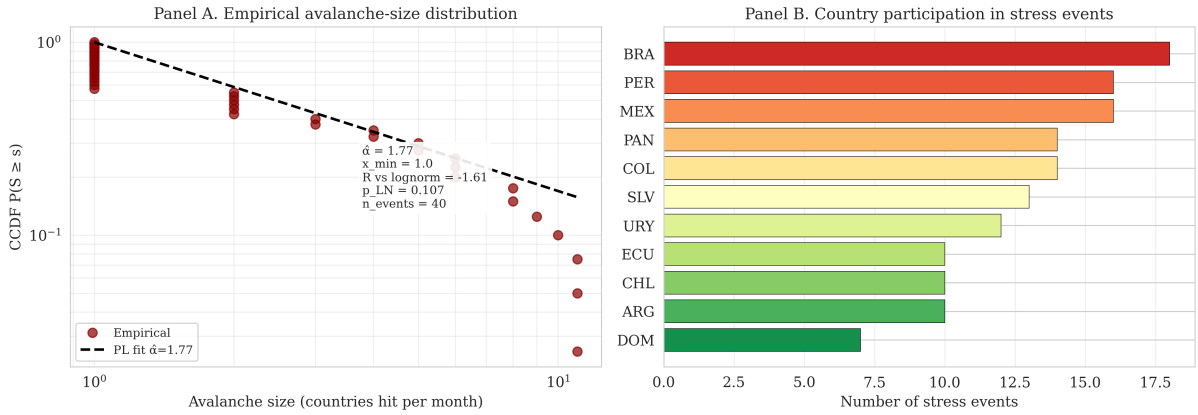


Figure 2: Empirical sovereign-stress avalanches in LATAM EMBI spreads. Panel A reports the avalanche-size CCDF with maximum-likelihood power-law fit ($\hat{\alpha} = 1.77$). Panel B reports country participation by stress-event count.

Figure 3 reports the corresponding diagnostic for pooled absolute monthly spread changes. This figure is not the primary SOC object, because the relevant propagation object is the synchronized avalanche size S_t . It is included to show that the underlying EMBI innovations are also heavy-tailed.

Figure 3. Tail diagnostic for monthly EMBI spread changes

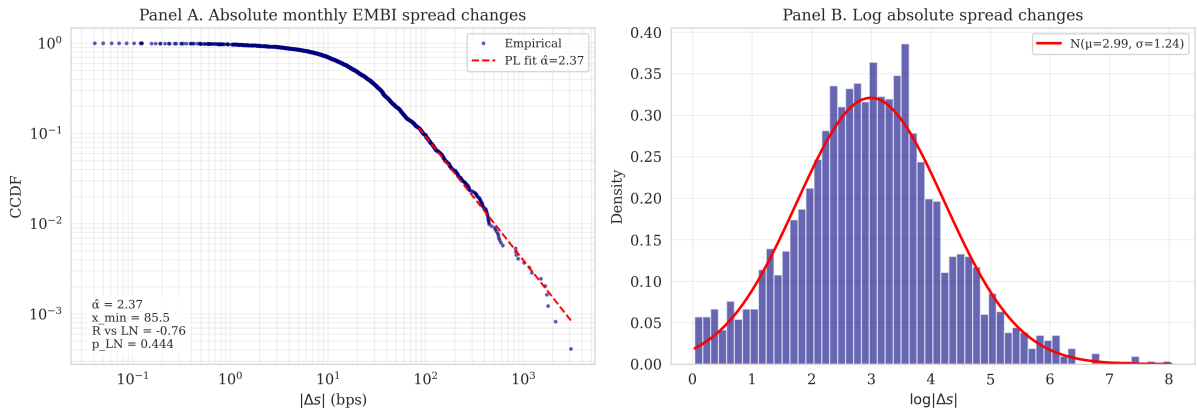


Figure 3: Tail diagnostic for monthly EMBI spread changes. Panel A reports pooled absolute monthly spread changes with power-law fit ($\hat{\alpha} = 2.37$, $x_{\min} \simeq 86$ basis points). Panel B reports the histogram of log-absolute spread changes with a normal overlay.

The estimated avalanche exponent lies in the range commonly associated with finite-size critical systems (Bak, 1996; Newman, 2005). However, because the lognormal alternative cannot be decisively ruled out and the number of tail observations is moderate, the interpretation is deliberately conservative: the evidence supports heavy-tailed finite-size avalanche behavior, not a claim of uniquely identified asymptotic self-organized criticality. **H1 is therefore confirmed in its conservative form: the distribution of sovereign-stress avalanche sizes is heavy-tailed and lies in a finite-size criti-**

cality regime, with an estimated exponent in the plausible critical range and lognormal alternatives not decisively preferred.

6.2 Non-random synchronization (H2)

Table 3 reports the country-level reshuffling placebo test. The placebo preserves each sovereign’s total number of stress events but randomizes the timing of those events within country. It therefore tests whether the observed avalanche sizes are mechanically generated by country-specific hit frequencies.

The observed maximum avalanche size is $\max_t S_t = 11$, whereas the placebo distribution has a mean maximum size of approximately 3.47 and a 95th percentile equal to 4. The observed share of large avalanches is also far above its placebo counterpart. All four synchronization statistics reject the reshuffled-timing null at $p < 0.001$. **This is the strongest result of the paper: regional EMBI stress synchronization is not an artifact of having several volatile countries in the same sample, and H2 is confirmed decisively.**

Table 3: Placebo test of cross-country stress synchronization. Country-level stress indicators are independently reshuffled across calendar months, destroying cross-country timing dependence while preserving country-level event frequencies.

Statistic	Observed	Placebo mean	Placebo P95	p -value
Max avalanche size S_{\max}	11	3.47	4.00	< 0.001
Mean positive avalanche size $\mathbb{E}[S \mid S > 0]$	3.50	1.32	1.40	< 0.001
Share $P(S \geq 4)$	0.350	0.005	0.019	< 0.001
Share $P(S \geq 6)$	0.250	0.000	0.000	< 0.001

Placebo replications: $B = 1,000$, seed = 2026.

The reshuffling placebo preserves each sovereign’s total number of stress events but destroys the common calendar timing of those events.

Under independent country-level stress timing, the mean placebo maximum avalanche size is 3.47 and the 95th percentile is 4. The observed value $S_{\max} = 11$ is not reached in any of the 1,000 placebo replications.

All four synchronization statistics reject the independent-timing null at $p < 0.001$, confirming that simultaneous LATAM sovereign stress is a non-trivial multi-country phenomenon.

It is important to be precise about what the placebo identifies. By construction, the test rules out the null in which country-level stress events are timed independently across sovereigns. It therefore demonstrates that the observed cross-sectional clustering is non-random conditional on country-specific event frequencies. The test does not separate two substantive sources of synchronization: endogenous regional propagation (stress in country i raising the probability of stress in country j) and exogenous common-factor synchronization (stress in country i and country j jointly responding to a global shock). The largest avalanches in the sample coincide with global systemic events, which suggests that common-factor synchronization plays a non-trivial role. The interpretation of the paper is consistent with this observation: the avalanche framework documents the

empirical existence of synchronized regional stress as a finite-size statistical phenomenon, without claiming to identify a unique structural transmission channel.

Table 4 lists the largest avalanche months and their historical interpretation. The three avalanches with $S_t = 11$ coincide with global systemic events: the Lehman collapse, the post-Lehman emerging-market rout, and the COVID-19 global financial shock. More broadly, the largest avalanches align with recognizable international stress episodes rather than with isolated country-specific spread events. This historical coherence supports the interpretation of S_t as a meaningful regional stress variable.

Table 4: Top 12 largest empirical avalanches in LATAM EMBI spreads, with historical context.

Rank	Month	S_t	Countries hit	Historical context
1	2020-03	11	ARG, BRA, CHL, COL, DOM, ECU, MEX, PAN, PER, SLV, URY	COVID-19 global rout, Ecuador default
2	2008-09	11	ARG, BRA, CHL, COL, DOM, ECU, MEX, PAN, PER, SLV, URY	Lehman collapse (global GFC peak)
3	2008-10	11	ARG, BRA, CHL, COL, DOM, ECU, MEX, PAN, PER, SLV, URY	Post-Lehman EM rout
4	2007-11	10	ARG, BRA, CHL, COL, DOM, MEX, PAN, PER, SLV, URY	Pre-crisis volatility wave (Bear Stearns hedge funds collapse)
5	2011-09	9	ARG, BRA, CHL, COL, MEX, PAN, PER, SLV, URY	Eurozone crisis intensifies
6	2010-05	8	BRA, CHL, COL, DOM, MEX, PER, SLV, URY	Eurozone crisis (first Greek bailout)
7	2012-05	8	ARG, BRA, CHL, COL, MEX, PAN, PER, URY	Greek collapse round II
8	2008-06	6	BRA, COL, MEX, PAN, PER, SLV	Subprime spillover to EM
9	2020-02	6	CHL, ECU, MEX, PAN, PER, URY	COVID-19 onset, Ecuador default brewing
10	2014-01	6	ARG, BRA, COL, MEX, PER, URY	EM Fragile Five sell-off
11	2011-08	5	BRA, CHL, COL, MEX, PAN	U.S. debt-ceiling / S&P downgrade
12	2022-06	5	BRA, COL, DOM, ECU, MEX	Fed front-loading; LATAM commodity stress

Each row is a calendar month ranked by $S_t =$ number of countries simultaneously exceeding their 1.5σ threshold.

Every avalanche of size $S \geq 9$ coincides with a documented global systemic event.

All $S = 11$ months are universal-stress events (every LATAM sovereign in the panel hit simultaneously).

6.3 Threshold robustness (H3)

Figure 4 and Table 5 examine whether the avalanche evidence depends on the baseline stress threshold $\sigma = 1.5$. The estimated avalanche exponent remains in a narrow range

for the empirically informative thresholds:

$$\hat{\alpha} \in [1.70, 1.83] \quad \text{for } \sigma \leq 2.00.$$

At higher thresholds, the number of avalanche months falls mechanically and tail estimates become less stable, as expected in a finite system. Importantly, the maximum avalanche size remains equal to eleven at every threshold in the grid. The largest regional stress events are therefore not artifacts of the baseline threshold choice.

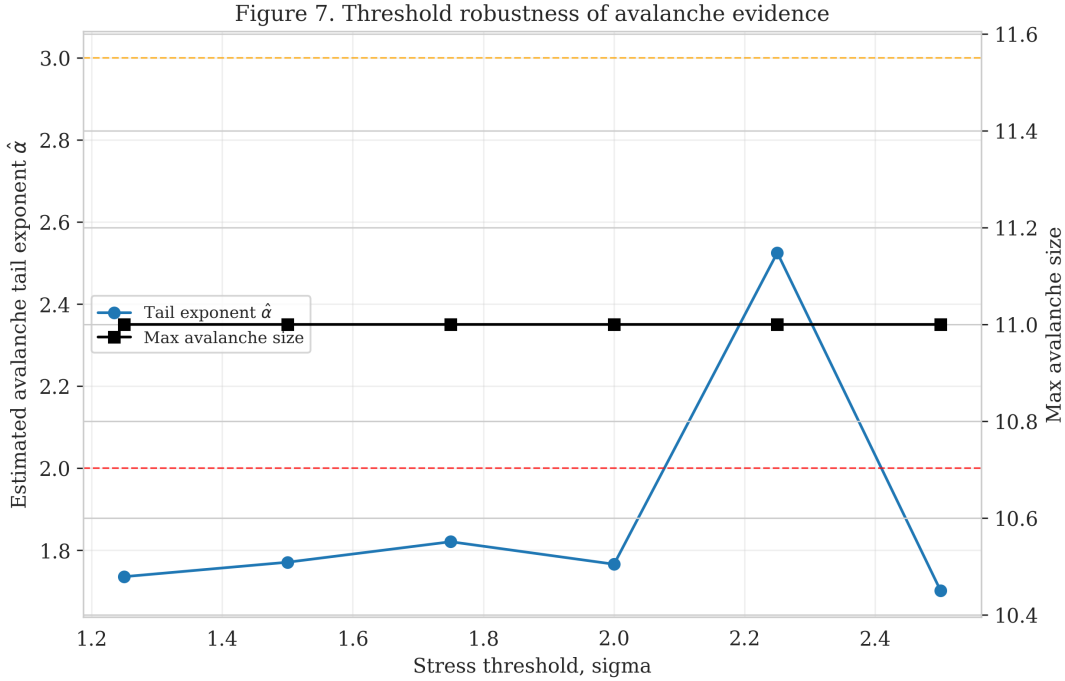


Figure 4: Threshold robustness of avalanche evidence. The blue line reports the estimated avalanche tail exponent $\hat{\alpha}$ on the left axis. The black line reports the maximum avalanche size on the right axis. Thresholds range from $\sigma = 1.25$ to $\sigma = 2.50$.

The robustness exercise supports the finite-size interpretation. The precise tail exponent varies with the threshold, but the existence of very large regional avalanches does not. This distinction matters because the central empirical claim is not tied to one arbitrary cutoff; it is the persistence of large synchronized events across reasonable event definitions. **H3 is therefore confirmed: the estimated tail exponent and maximum avalanche size are stable across the empirically informative threshold range.**

6.4 Heterogeneous country participation (H4)

Table 6 reports the country-specific stress thresholds and event counts. Stress participation is highly heterogeneous. Brazil records the largest number of stress events, followed by Mexico and Peru, while the Dominican Republic records the fewest. A χ^2 test against

Table 5: Sensitivity of avalanche evidence to the stress-threshold parameter σ .

σ	Country hits	Avalanche months	Mean S	Max S	$P(S \geq 6)$	$\hat{\alpha}$	x_{\min}	$R_{\text{PL/LN}}$	p_{LN}
1.25	199	54	3.69	11	0.241	1.736	1.000	-2.106	0.035
1.50	140	40	3.50	11	0.250	1.771	1.000	-1.612	0.107
1.75	112	35	3.20	11	0.171	1.821	1.000	-1.393	0.164
2.00	67	19	3.53	11	0.263	1.766	1.000	-1.181	0.238
2.25	52	13	4.00	11	0.308	2.525	4.000	-1.005	0.315
2.50	41	10	4.10	11	0.300	1.702	1.000	-0.878	0.380

Avalanche months are months with $S_t > 0$. Mean S denotes the average avalanche size conditional on an avalanche occurring.

The main qualitative conclusion is robust across thresholds: universal avalanches with $S_{\max} = 11$ appear at every tested value of σ .

Tail-exponent stability is strongest over the empirically informative range $\sigma \leq 2.00$, where $\hat{\alpha} \in [1.70, 1.83]$.

At higher thresholds, the number of avalanche months falls mechanically and tail estimates become less stable, as expected in a finite-size system.

The likelihood-ratio evidence should be interpreted conservatively: at $\sigma = 1.25$, the lognormal alternative is favored at conventional significance levels, while for the baseline and higher thresholds it is not decisively preferred.

uniform participation rejects equality of stress frequencies across countries, indicating that avalanche participation is not evenly distributed across the regional system.

Table 6: Country-specific stress thresholds and observed event counts, $\sigma = 1.5$ specification

Code	Country	$\sigma_{\Delta \log s}$	Threshold	N_c	Hit rate	Mean $ \Delta s $ (bp)	P95 $ \Delta s $ (bp)	Max $ \Delta s $ (bp)
BRA	Brazil	0.111	0.166	18	0.081	22	63	138
MEX	Mexico	0.109	0.163	16	0.072	22	62	281
PER	Peru	0.135	0.203	16	0.072	20	50	203
COL	Colombia	0.131	0.197	14	0.063	24	61	213
PAN	Panama	0.129	0.193	14	0.063	20	54	207
SLV	El Salvador	0.119	0.179	13	0.059	53	178	431
URY	Uruguay	0.136	0.203	12	0.054	22	63	421
ARG	Argentina	0.166	0.249	10	0.045	132	441	1,751
CHL	Chile	0.117	0.175	10	0.045	15	37	142
ECU	Ecuador	0.195	0.293	10	0.045	153	448	3,087
DOM	Dom. Rep.	0.119	0.178	7	0.032	37	91	1,018

Notes: A stress event for country c at month t is defined by $\Delta \log s_{c,t} > \sigma \cdot \hat{\sigma}_c$, where $\hat{\sigma}_c$ is the country-specific standard deviation of monthly log changes.

Countries with the largest tail jumps, especially Argentina and Ecuador, display fewer events because their volatility is concentrated in a small number of regime-defining episodes.

Mid-credibility and highly traded sovereigns, especially Brazil, Mexico, Peru, Colombia, and Panama, accumulate the largest event counts.

The substantive result is that avalanche participation is not mechanically ordered by average spread level. Argentina and Ecuador are among the highest-spread sovereigns in the panel, but they do not dominate the stress-event count. By contrast, more liquid and financially integrated sovereigns such as Brazil, Mexico, Peru, Colombia, and

Panama participate more frequently in regional stress episodes. This pattern is consistent with a network-amplification interpretation: the most frequently activated nodes are not necessarily the weakest sovereigns, but those that are sufficiently liquid, investable, and integrated into the regional emerging-market debt portfolio to react repeatedly to changes in global risk conditions.

Figures 5 and 6 display the timing of country-level stress recurrence. The largest clusters occur around the global financial crisis and the COVID-19 shock, with additional stress episodes in 2010–2011 and during selected emerging-market repricing periods. The temporal pattern reinforces the interpretation that country participation is shaped by regional and global synchronization, not only by idiosyncratic fiscal weakness. **H4 is therefore confirmed: country participation is heterogeneous and is not mechanically ordered by average spread level.**

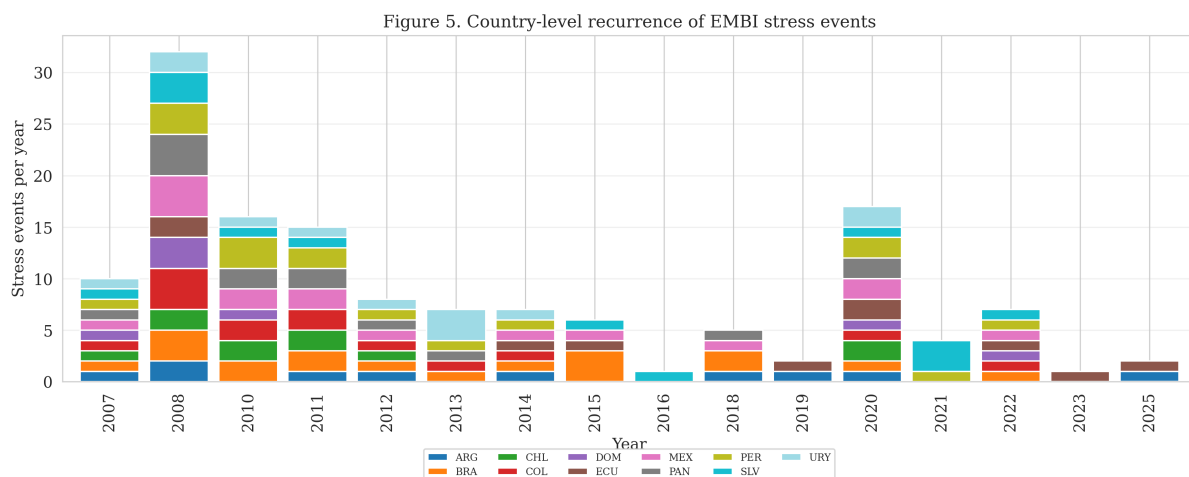


Figure 5: Country-level recurrence of EMBI stress events by year, stacked across countries. The largest cluster occurs in 2008, followed by stress clusters around 2010–2011 and 2020.

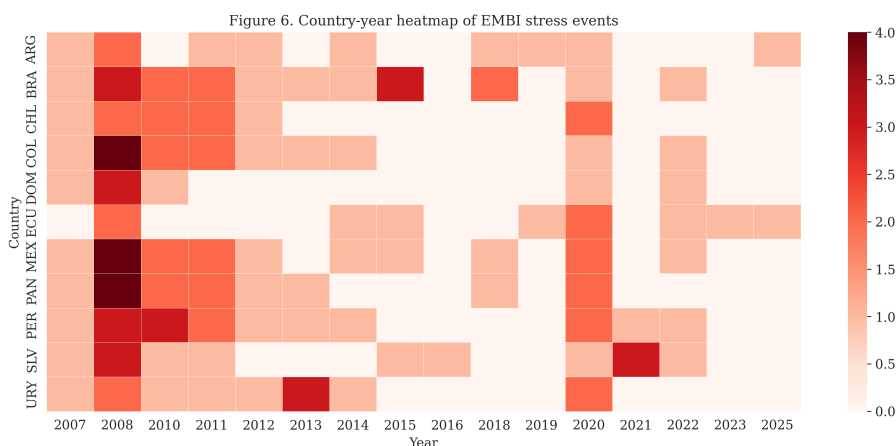


Figure 6: Country-year heatmap of EMBI stress events. Cell intensity reports the number of months in which country c exceeded its 1.5σ stress threshold in year y .

6.5 Network amplification during large avalanches (H5)

Figure 7 displays the three filtered co-movement networks at four representative dates. The correlation network becomes extremely dense in systemic periods, reflecting common regional repricing. The partial-correlation network is sparser and more informative about conditional co-movement after filtering common linear dependence. The minimum spanning tree provides a fixed-edge benchmark for the strongest hierarchical co-movement structure.

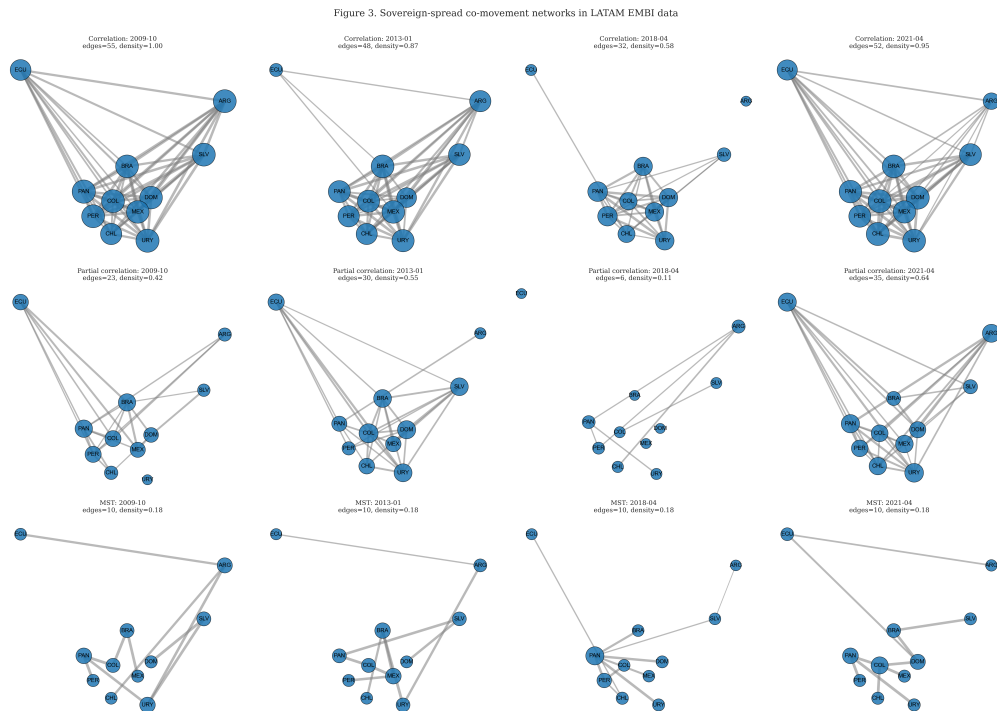


Figure 7: Sovereign-spread co-movement networks in LATAM EMBI data at four representative dates. Top row: correlation network. Middle row: partial-correlation network. Bottom row: minimum spanning tree.

Figure 8 traces the dynamics of network amplification and geometry. The most economically informative panels are the normalized spectral radius, the Spectral Fragility Index, and network density. Curvature measures are reported as auxiliary geometric indicators, while spectral metrics are the main measures of amplification.

Figure 4. Network amplification and geometry in LATAM EMBI spreads



Figure 8: Network amplification and geometry in LATAM EMBI spreads, 2009–2026. The figure reports curvature, normalized spectral radius, Spectral Fragility Index, and density across correlation, partial-correlation, and minimum spanning tree filters.

Table 7 compares network metrics in 24-month windows containing at least one large avalanche ($S_t \geq 6$) with windows that do not. The evidence on regime differences is heterogeneous across filters and deserves a careful reading.

The correlation network displays the largest and most statistically significant regime differences. Network density rises from 0.74 in non-large windows to 0.92 in large-avalanche windows ($t = 5.42$, $p < 0.001$), and the maximum-row-sum normalized spectral radius rises from 0.85 to 0.91 ($t = 6.26$, $p < 0.001$). The corresponding maximum-row-sum SFI rises from 6.23 to 11.74, and the Frobenius SFI from 11.86 to 16.30. The HHI of node strength falls in large-avalanche windows ($t = -4.65$, $p < 0.001$), indicating that regional stress connectivity becomes both more amplifying and more evenly distributed across sovereigns. The minimum spanning tree shows mixed but smaller regime differences, reflecting the constraint of a fixed edge count.

The partial-correlation network, by contrast, does *not* display significant regime differences in any of its spectral or density metrics. The maximum-row-sum spectral radius is essentially flat (0.871 versus 0.855, $p = 0.435$), the Frobenius spectral radius is mildly lower in large-avalanche windows (0.914 versus 0.896, $p = 0.144$), and the corresponding SFI measures show no statistically significant change. Density rises only marginally (0.69

to 0.72, $p = 0.651$).

This contrast is informative rather than contradictory. Raw correlation networks become denser and more spectrally amplifying around large avalanches, but raw correlations are known to rise mechanically during high-volatility episodes (Forbes and Rigobon, 2002). Partial correlations filter the common linear factor that drives this mechanical effect. The fact that partial-correlation networks do not exhibit additional spectral amplification in large-avalanche windows therefore suggests that most of the observed network-amplification signal in raw correlations is attributable to common-factor co-movement rather than to genuine increases in conditional regional propagation. **H5 is therefore partially confirmed: large avalanche regimes are associated with denser and more amplifying network states in the correlation filter, but this regime difference is not robust to partial-correlation filtering.** The substantive interpretation is that amplification in EMBI co-movement networks during large avalanches is predominantly a common-factor phenomenon rather than a conditional-network phenomenon.

6.6 Lead–lag network association (H6)

Table 8 reports lead–lag associations between contemporaneous network metrics and the maximum avalanche size over the subsequent three months, $Y_t = \max_{u \in (t, t+3]} S_u$. The results are not interpreted as causal estimates. They are intended to evaluate whether network states contain early-warning information about near-future regional stress.

The empirical evidence on lead–lag predictability is weak. None of the network metrics in any of the three filters yields a Pearson correlation that is statistically significant at conventional levels. The largest absolute correlation is observed for the maximum-row-sum spectral radius of the correlation network, $r = +0.153$ ($p = 0.217$), which suggests a positive but imprecisely estimated association. The corresponding metrics in the partial-correlation network are smaller in absolute value and not statistically distinguishable from zero, with the Frobenius spectral radius giving $r = -0.097$ ($p = 0.436$) and the Frobenius SFI giving $r = -0.073$ ($p = 0.555$). The minimum spanning tree shows similarly weak associations.

The point estimates are also small in economic terms. With $n = 67$ rolling network snapshots, even the strongest observed correlation explains less than 3 percent of the variance in three-month-ahead maximum avalanche size. H6 is therefore not supported by the data: contemporaneous network metrics do not provide statistically significant predictive content for near-future regional stress at the three-month horizon in this sample.

This null result deserves direct discussion rather than being explained away. Three considerations are relevant. First, the predictive horizon and sample size are modest: with monthly rolling windows and a forecast horizon of three months, the effective number of independent observations available for inference is small, and statistical power is limited.

Table 7: Network geometry around large stress months. Welch’s two-sample t -test contrasts metric values in 24-month rolling windows containing a large avalanche ($S \geq 6$) versus all other windows.

Filter	Metric	Non-large mean	Large mean	Δ	t	p	n_L	n_N
corr	ρ^{\max}	0.847	0.911	0.065	6.259	0.000	33	34
corr	ρ^{Fro}	0.913	0.941	0.027	4.607	0.000	33	34
corr	SFI^{\max}	6.229	11.743	5.515	6.304	0.000	33	34
corr	SFI^{Fro}	11.858	16.296	4.438	5.636	0.000	33	34
corr	$\bar{\kappa}^O$	0.935	0.963	0.028	4.132	0.000	33	34
corr	$\bar{\kappa}^F$	1.138	1.254	0.116	2.547	0.014	33	34
corr	Density	0.739	0.915	0.177	5.419	0.000	33	34
corr	HHI strength	0.106	0.096	-0.010	-4.645	0.000	33	34
partial	ρ^{\max}	0.871	0.855	-0.015	-0.786	0.435	33	34
partial	ρ^{Fro}	0.914	0.896	-0.018	-1.480	0.144	33	34
partial	SFI^{\max}	10.079	10.173	0.093	0.044	0.965	33	34
partial	SFI^{Fro}	12.696	11.159	-1.537	-1.244	0.219	33	34
partial	$\bar{\kappa}^O$	0.923	0.909	-0.014	-0.878	0.383	33	34
partial	$\bar{\kappa}^F$	1.262	1.230	-0.032	-0.533	0.596	33	34
partial	Density	0.693	0.715	0.023	0.454	0.651	33	34
partial	HHI strength	0.109	0.106	-0.004	-1.262	0.211	33	34
mst	ρ^{\max}	0.562	0.614	0.052	2.832	0.006	33	34
mst	ρ^{Fro}	0.558	0.516	-0.042	-6.453	0.000	33	34
mst	SFI^{\max}	1.336	1.721	0.385	2.988	0.004	33	34
mst	SFI^{Fro}	1.270	1.074	-0.195	-6.235	0.000	33	34
mst	$\bar{\kappa}^O$	0.812	0.874	0.061	4.510	0.000	33	34
mst	$\bar{\kappa}^F$	1.445	1.689	0.245	6.208	0.000	33	34
mst	HHI strength	0.135	0.119	-0.016	-5.930	0.000	33	34

Filters refer to the network construction: $|\rho| > 0.4$ (corr), $|\rho^{\text{part}}| > 0.4$ (partial), or the minimum-spanning-tree filter (mst).

Network density and edge counts in the MST are constant by construction, with 10 edges among 11 nodes, and are therefore omitted.

The correlation network exhibits the strongest large-vs-non-large discrimination: density, spectral radius, SFI, and curvature increase significantly during large-avalanche windows, while node-strength concentration falls.

Partial-correlation metrics do not display statistically significant regime differences, suggesting that the raw-correlation amplification signal is mainly driven by common-factor comovement rather than conditional regional propagation.

MST metrics show statistically significant but mixed regime differences and should be interpreted as a sparse topological benchmark rather than as the main amplification evidence.

Table 8: Lead–lag association between current network geometry and the maximum avalanche size over the next three months.

Filter	Metric	Pearson r	p	n
corr	ρ^{\max}	+0.153	0.217	67
corr	ρ^{Fro}	+0.094	0.448	67
corr	SFI^{\max}	+0.080	0.518	67
corr	SFI^{Fro}	+0.077	0.537	67
corr	$\bar{\kappa}^{\mathcal{O}}$	+0.027	0.826	67
corr	Density	+0.117	0.345	67
corr	HHI strength	-0.128	0.304	67
partial	ρ^{\max}	-0.117	0.347	67
partial	ρ^{Fro}	-0.097	0.436	67
partial	SFI^{\max}	+0.021	0.867	67
partial	SFI^{Fro}	-0.073	0.555	67
partial	$\bar{\kappa}^{\mathcal{O}}$	-0.040	0.749	67
partial	Density	-0.006	0.960	67
partial	HHI strength	-0.038	0.758	67
mst	ρ^{\max}	+0.121	0.329	67
mst	ρ^{Fro}	-0.059	0.638	67
mst	SFI^{\max}	+0.132	0.287	67
mst	SFI^{Fro}	-0.053	0.672	67
mst	$\bar{\kappa}^{\mathcal{O}}$	+0.063	0.613	67
mst	HHI strength	-0.060	0.631	67

Each row reports the Pearson correlation between a network metric at month t and $\max_{u \in (t, t+3]} S_u$.

No network metric displays a statistically significant three-month-ahead association with future maximum avalanche size.

The largest absolute correlation is modest, $|r| = 0.153$, and all reported p -values exceed conventional significance levels.

MST metrics should be interpreted cautiously because the minimum-spanning-tree filter imposes a fixed-edge topology.

Second, the finding is consistent with the regime-comparison evidence in Section 6.5: most of the network signal around large avalanches reflects common-factor co-movement, which is contemporaneous with stress rather than a leading indicator of it. Third, the result does not preclude predictive content at different horizons, with different network filters, or in specifications that combine network information with global risk variables. A richer multivariate predictive model is left to future work.

The conservative reading is that the network evidence in this paper identifies a contemporaneous regime structure (Section 6.5) but does not establish a robust early-warning signal at the three-month horizon. Operationally, this means that the avalanche-size process S_t and the placebo-validated synchronization evidence remain the primary surveillance objects of the paper, while network amplification metrics are best interpreted as descriptive features of stress regimes rather than as predictive instruments.

6.7 Summary of findings

Table 9 summarizes the six empirical hypotheses in the order in which they were stated in Section 3. The evidence supports the presence of heavy-tailed finite-size avalanches (H1), non-random synchronization (H2), threshold robustness over the informative range (H3), and heterogeneous country participation (H4). The evidence on network amplification during large avalanches (H5) is partially supportive, with the correlation filter showing strong regime differences but the partial-correlation filter showing none, suggesting that the regime difference reflects common-factor co-movement rather than conditional network amplification. The evidence on predictive lead-lag network association (H6) is not supportive at the three-month horizon in this sample. The strongest results of the paper are therefore the synchronization placebo and the threshold-robust existence of large regional avalanches.

Overall, the empirical results indicate that Latin American sovereign credit markets exhibit finite-size avalanche dynamics. The system is not merely a collection of independent national spread shocks. Large regional stress episodes are synchronized beyond country-level hit frequencies, appear in historically meaningful periods, and are associated with denser correlation network states during stress regimes. The evidence is therefore consistent with a finite-size criticality interpretation of LATAM sovereign stress in its avalanche-size and synchronization dimensions, while the network-amplification dimension is more conditional: it is detectable in raw co-movement but not robust to partial-correlation filtering, and it does not deliver statistically significant lead-lag predictive content at the three-month horizon. The paper therefore claims a heavy-tailed, synchronized, and historically coherent regional stress process, while remaining cautious about the stronger claims of conditional network amplification and network-based early warning.

Table 9: Summary of hypotheses, tests, and outcomes.

#	Hypothesis	Test / evidence	Outcome
H1	Avalanche-size distribution is heavy-tailed and lies in a finite-size criticality regime.	Clauset MLE + Vuong test; Table 2; Fig. 2.	Confirmed in conservative form; $\hat{\alpha} = 1.77$, $x_{\min} = 1$, and the lognormal alternative is not decisively preferred.
H2	Cross-country sovereign-stress synchronization is non-random.	Country-level reshuffling placebo, $B = 1,000$; Table 3.	Confirmed decisively; observed $S_{\max} = 11$ is far above the placebo distribution, with $p < 0.001$ for all synchronization statistics.
H3	Avalanche evidence is robust to the choice of stress threshold σ .	Threshold sensitivity over $\sigma \in [1.25, 2.50]$; Table 5; Fig. 4.	Confirmed over the informative range; $\hat{\alpha} \in [1.70, 1.83]$ for $\sigma \leq 2.0$, and $S_{\max} = 11$ for all tested thresholds.
H4	Country-level participation in stress avalanches is heterogeneous and not mechanically ordered by average spread levels.	Country event counts; Table 6; Fig. 5–6.	Confirmed; participation ranges from 7 to 18 events, with Brazil, Mexico, Peru, Colombia, and Panama among the most recurrent participants.
H5	Large-avalanche windows are associated with more amplifying contemporaneous network states.	Regime comparison between large-avalanche and non-large-avalanche windows; Table 7; Fig. 8.	Partially confirmed; raw correlation networks become denser and more spectrally amplifying, but the result is not robust to partial-correlation filtering.
H6	Network amplification contains predictive lead-lag information for near-future regional stress.	Three-month-ahead Pearson correlations and OLS associations; Table 8.	Not supported; no network metric is statistically significant at the three-month horizon in any filter.

All tests are based on monthly EMBI Global Diversified stripped spreads for 11 LATAM countries over 2007:M10–2026:M4.

The heavy-tail evidence is interpreted conservatively as finite-size criticality evidence, not as proof of a unique asymptotic power law.

The mid-credibility result is treated as part of H4’s substantive interpretation rather than as a separate formal hypothesis.

7 Discussion

The empirical results position Latin American sovereign credit markets in a finite-size heavy-tail regime. The evidence is not strong enough to claim that EMBI spreads obey a unique asymptotic power law, nor that Latin American sovereign risk is a pure self-organized critical system. However, the results are clearly inconsistent with a thin-tailed, independent-country interpretation of sovereign stress. Large regional avalanches occur substantially more frequently than would be expected under country-level stress frequencies alone, and these avalanches occur in contemporaneous network environments that are denser and more spectrally integrated. The relevant interpretation is therefore one of finite-size criticality: a bounded regional system in which stress is episodic, synchronized, heavy-tailed, and embedded in a time-varying co-movement structure that amplifies common shocks. The paper is also explicit about what the network evidence does not establish, in particular the absence of significant lead-lag predictive content at the three-month horizon and the absence of regime differences once partial-correlation filtering removes common-factor co-movement.

7.1 Implications for surveillance

The first implication concerns sovereign-risk surveillance. Standard monitoring frameworks focus on country-level fundamentals: debt ratios, primary balances, reserves, current-account positions, inflation, rollover needs, and political risk. These variables remain essential, but the evidence in this paper suggests that they should be complemented by regional synchronization indicators. The avalanche-size process S_t provides a simple, computationally inexpensive measure of how many sovereigns are simultaneously experiencing large spread innovations, and its empirical distribution and historical alignment with global systemic events make it a meaningful regional stress-state variable.

The role of network metrics in this surveillance framework requires more careful articulation than the paper initially anticipated. The regime-comparison evidence in Table 7 shows that the raw correlation network discriminates large-avalanche from non-large-avalanche windows with high statistical significance: density, the maximum-row-sum spectral radius, the Spectral Fragility Index, and the inverse of node-strength concentration all move sharply when the regional system enters a stress regime. The partial-correlation network, by contrast, does not discriminate regimes in any of its spectral or density metrics. The substantive interpretation of this asymmetry is that most of the network amplification observed during large avalanches reflects common-factor co-movement of the type emphasized by [Forbes and Rigobon \(2002\)](#), rather than additional conditional regional propagation. Once the common linear factor is filtered out, the network no longer becomes more amplifying around stress episodes.

This finding does not eliminate the operational usefulness of the SFI; it clarifies what

kind of usefulness it has. The SFI on the raw correlation network behaves as a contemporaneous descriptor of regional stress regimes, in the same way that realized volatility, implied volatility, or the breadth of asset-class drawdowns are contemporaneous descriptors of financial conditions. The lead–lag analysis in Table 8 reinforces this contemporaneous interpretation: no network metric, in any of the three filters, exhibits a statistically significant correlation with three-month-ahead maximum avalanche size. The largest absolute correlation in the table is $r = +0.153$ for the maximum-row-sum spectral radius of the correlation network, with $p = 0.217$. This null result deserves direct acknowledgment rather than rationalization: the network metrics in this sample are informative about contemporaneous stress regimes, but they do not deliver robust early-warning signals at the three-month horizon.

In practice, this means that monthly SFI nowcasts can be computed at low cost from rolling EMBI spread changes and used as an additional layer of contemporaneous regional stress monitoring by central banks, multilateral institutions, and sovereign-risk teams. They should not be interpreted as forecasts of crisis. Their role is closer to that of a thermometer than that of a barometer: they describe the current temperature of the regional stress system rather than predict where it is going. For genuine early-warning content, future work would need to combine network metrics with other variables—global risk appetite indices, U.S. monetary-policy indicators, commodity prices, and country-level fundamentals—in a richer multivariate framework that the present paper does not attempt.

7.2 Regional political economy of sovereign fragility

The second implication concerns the political economy of regional fragility. A conventional weak-link view would suggest that the most fragile countries are the highest-spread sovereigns. Under that interpretation, Argentina and Ecuador should dominate the stress-event process. The data do not support that view. These countries display very high spread levels and extreme regime-defining episodes, but they do not generate the largest number of threshold crossings. Their stress is episodic and discontinuous: defaults, currency collapses, and restructuring episodes can push spreads into high absorbed states, after which additional monthly threshold crossings become less frequent.

By contrast, countries such as Brazil, Mexico, Peru, Colombia, and Panama participate more frequently in regional stress events. These sovereigns are not necessarily the highest-risk economies in average spread terms, but they are more liquid, more investable, and more central in global emerging-market portfolios. Their spreads respond repeatedly to changes in global risk appetite, monetary tightening, benchmark rebalancing, and regional investor coordination. The implication is that Latin American sovereign fragility is not only the fragility of its weakest fiscal links. It is also the fragility of its capital-market

integration as a system. The countries that matter most for regional avalanches may be those that sit at the intersection of credibility, liquidity, and exposure to global portfolio adjustment.

This interpretation is reinforced by the partial-correlation regime result. If the network amplification observed during large avalanches were driven primarily by structural regional propagation, conditional co-movement should rise during stress episodes. The fact that it does not—while raw co-movement does—is consistent with the view that the mid-credibility, highly-integrated sovereigns participate in regional stress because they jointly absorb global shocks rather than because they transmit shocks to one another in conditional terms. Latin American sovereign credit markets behave, during stress regimes, more as a single asset class facing a common factor than as a network of bilateral propagation channels.

This distinction is important for policy interpretation. A surveillance framework focused only on fiscal weakness may identify countries with high default risk but miss the countries that most strongly synchronize regional stress through their integration into global emerging-market portfolios. Conversely, a network-based framework that emphasizes conditional regional propagation may overstate the role of bilateral transmission relative to common-factor exposure. For regional financial stability, the relevant question is therefore not only which country is fiscally weakest, but which sovereigns are positioned to convert global risk shocks into regional co-movement, and what fraction of regional synchronization is structural versus common-factor in nature.

7.3 Criticality as a system-level property

The third implication is theoretical. The results suggest that criticality in sovereign credit markets is a system-level phenomenon rather than a smooth aggregation of country-level properties. Additional country-level diagnostics show that the association between country-specific recurrence exponents and country-level curvature is weak and statistically insignificant. This finding is not a failure of the framework. It is consistent with the logic of sandpile-type systems, where critical behavior is not a property of isolated sites but an emergent feature of the interaction structure.

In the present context, no single country needs to display a stable curvature–exponent relationship for the regional system to generate heavy-tailed avalanches. What matters is the configuration of thresholds, market integration, common shocks, and conditional co-movement. Large avalanches emerge when enough countries are simultaneously close to their stress thresholds and are jointly exposed to a sufficiently strong common factor. This is why the paper emphasizes system-level objects— S_t , density, spectral radius, SFI, and the placebo synchronization test—rather than relying on country-level tail estimates alone.

This interpretation also clarifies the role of curvature. The empirical Ollivier–Ricci and Forman–Ricci curvature measures are useful as geometric summaries of network integration, but they should not be treated as the central fragility indicator in this application. In dense sovereign-spread networks, positive curvature may reflect redundant co-movement rather than bottleneck fragility. The main operational measures of amplification are therefore spectral: the normalized spectral radius and the corresponding Spectral Fragility Index. These measures connect more directly to the propagation dynamics and to the stability boundary of linearized network systems, even if their predictive content in this sample is contemporaneous rather than leading.

7.4 Limitations and extensions

Several limitations qualify the interpretation. First, EMBI spreads are secondary-market price indicators. They capture sovereign credit risk as priced by investors, but they do not directly observe bond flows, foreign holdings, dealer balance sheets, issuance quantities, or primary-market funding costs. The avalanche process identified here is therefore an asset-price stress process, not a full balance-sheet contagion mechanism.

Second, the network is inferred from rolling co-movement in monthly spread changes. This is appropriate for a long regional panel, but it cannot fully separate structural transmission from common shocks, portfolio rebalancing, or global risk-appetite shifts. The partial-correlation network reduces this problem and, as discussed above, the comparison between the two filters is itself informative about the common-factor versus conditional-network decomposition. Future work could combine EMBI spreads with fund-flow data, mutual-fund holdings, sovereign issuance calendars, or high-frequency CDS data to better identify transmission channels and to test whether the common-factor interpretation continues to dominate at higher frequencies.

Third, the analysis is finite-sample by construction. The system contains only eleven sovereigns, the monthly sample covers 223 periods, and the number of avalanche events above the estimated power-law cutoff is moderate. This is adequate for documenting finite-size avalanche behavior and non-random synchronization, but it limits the ability to distinguish cleanly between power-law, lognormal, and other heavy-tailed alternatives, and it limits the power of the lead–lag predictive analysis. For this reason, the paper does not claim to prove an asymptotic SOC law, and it does not interpret the null lead–lag result as definitive evidence against predictive content; both conclusions are constrained by sample size.

Fourth, the MST filter is intentionally sparse and has a fixed number of edges. This makes it useful as a topological benchmark but limits its ability to capture high-density stress regimes. Richer filtering methods, such as planar maximally filtered graphs (Tuminello et al., 2005), graphical lasso networks, dynamic factor-adjusted networks, or

time-varying parameter VAR connectedness models, could provide additional robustness. Similarly, the 24-month rolling window used here balances precision and responsiveness, but future work could validate the results using weekly or daily EMBI/CDS data, where the contemporaneous-versus- predictive distinction can be sharpened.

7.5 What the paper does and does not establish

It is useful to state the interpretive boundaries of the paper directly. The paper establishes that LATAM sovereign credit markets exhibit heavy-tailed finite-size avalanche behavior, threshold-robust large regional stress events, and synchronization that is far stronger than what would be achievable under independent country-level timing. It establishes that participation in these avalanches is dominated by mid-credibility, highly integrated sovereigns rather than by the highest-spread economies. It establishes that the contemporaneous co-movement network becomes denser and more spectrally amplifying during stress regimes when measured by raw correlations.

The paper does not establish that EMBI spreads obey a unique asymptotic power law, that the avalanche process is governed by a pure SOC mechanism, or that conditional regional propagation increases significantly during stress regimes once common-factor co-movement is filtered out. It does not establish a statistically significant lead-lag predictive relationship between network metrics and regional stress at the three-month horizon. These boundaries are not weaknesses of the analysis. They define the empirical content of the paper precisely: a disciplined, finite-sample documentation of heavy-tailed and synchronized sovereign stress in a region for which such evidence has not previously been assembled.

Overall, the evidence supports a disciplined interpretation: Latin American sovereign credit markets display finite-size criticality signatures, but not a uniquely identified pure SOC law. The system generates large synchronized stress avalanches, these avalanches are historically meaningful and statistically non-random, and their occurrence coincides with denser regional co-movement networks. This combination of results suggests that sovereign-risk surveillance should move beyond country-by-country spread monitoring toward a regional view of stress synchronization and contemporaneous network state.

8 Conclusion

This paper studies whether Latin American sovereign credit markets exhibit empirical signatures of finite-size criticality. Using monthly J.P. Morgan EMBI Global Diversified stripped spreads for eleven Latin American economies from October 2007 to April 2026, the paper constructs country-level stress events from threshold exceedances in monthly log-spread changes and defines regional sovereign-stress avalanches as the number of coun-

tries simultaneously in stress. The analysis combines heavy-tail diagnostics, threshold robustness checks, reshuffling placebos, rolling co-movement networks, spectral amplification measures, and lead–lag network associations.

The evidence supports a conservative but economically meaningful conclusion: Latin American sovereign spreads do not behave as a collection of independent country-level shocks. Instead, regional stress appears as a synchronized and heavy-tailed process embedded in a time-varying co-movement environment. Avalanche sizes exhibit a heavy-tailed distribution with an estimated exponent in the finite-size criticality range. Absolute spread changes and inter-event times also fall within a heavy-tail boundary regime in the sense of [Stumpf and Porter \(2012\)](#): power-law and lognormal specifications cannot be sharply separated in finite samples, but thin-tailed alternatives are inconsistent with the observed patterns. The results therefore do not prove a pure asymptotic self-organized critical law. They provide evidence that LATAM sovereign credit markets display finite-size avalanche dynamics consistent with critical propagation.

The strongest empirical result is the synchronization placebo. Preserving each country’s stress frequency but randomly reshuffling stress timing within country generates substantially smaller avalanches than those observed in the data, with $p < 0.001$ across all four synchronization statistics. This indicates that large regional sovereign-stress episodes are not a mechanical consequence of having volatile countries in the sample. They are temporally organized events. The largest avalanches coincide with historically meaningful episodes such as the Lehman collapse, the post-Lehman emerging-market rout, and the COVID-19 shock, reinforcing the interpretation of S_t as a regional stress-state variable.

The network results add a contemporaneous regime dimension that requires careful articulation. Large avalanche regimes are associated with denser and more spectrally amplifying co-movement networks when measured by raw correlations. However, this regime difference is not robust to partial-correlation filtering: once the common linear factor is removed, the spectral and density metrics no longer discriminate large-avalanche from non-large-avalanche windows. The substantive interpretation is that the observed network amplification reflects common-factor co-movement rather than additional conditional regional propagation, consistent with the well-known sensitivity of raw correlations to high-volatility episodes ([Forbes and Rigobon, 2002](#)). Lead–lag associations between contemporaneous network metrics and three-month-ahead maximum avalanche size are not statistically significant in any of the three network filters, with the largest absolute Pearson correlation reaching only $r = +0.153$ ($p = 0.217$). The Spectral Fragility Index and related metrics are therefore best interpreted as descriptors of contemporaneous regional stress regimes rather than as early-warning instruments at the three-month horizon.

The results also revise the political economy interpretation of sovereign fragility in Latin America. Regional stress is not driven only by the highest-spread or most fiscally

distressed sovereigns. Countries such as Brazil, Mexico, Peru, Colombia, and Panama participate frequently in stress events because they are liquid, investable, and deeply connected to global emerging-market portfolio dynamics. Argentina and Ecuador remain important high-risk sovereigns, but their stress episodes are more discontinuous and regime-specific. The relevant source of regional fragility is therefore not only weak fiscal fundamentals at the periphery; it is also the systemic integration of mid-credibility sovereigns into a common market for emerging-market credit risk. The asymmetry between the correlation and partial-correlation regime results reinforces this reading: regional fragility appears as the joint exposure of integrated sovereigns to a common risk factor, rather than as the product of dense bilateral propagation channels.

The contribution of the paper is methodological and empirical. Methodologically, it provides a framework for measuring sovereign-stress avalanches, testing whether synchronization exceeds country-level stress frequencies, and characterizing the contemporaneous network environment of regional stress regimes. The disciplined separation between correlation and partial-correlation filters, and between contemporaneous regime comparisons and lead-lag predictive associations, is itself a methodological contribution: it shows how to extract honest empirical content from network metrics in a setting where common-factor exposure is a dominant force. Empirically, it shows that LATAM EMBI spreads display finite-size avalanche behavior, threshold-robust large synchronized events, and contemporaneous network states that become more correlation-dense around systemic episodes. This complements standard sovereign-spread models based on fundamentals, liquidity, and global risk appetite by adding a regional dynamic layer: the same country-level fundamentals may generate different systemic outcomes depending on the contemporaneous state of the sovereign co-movement network.

The findings are relevant for surveillance. Central banks, multilateral institutions, and sovereign-risk analysts typically monitor country-level spreads, fiscal indicators, external balances, and rollover needs. The results suggest that these indicators should be complemented by system-level measures: the avalanche-size process, the frequency of large synchronized events, and contemporaneous network descriptors such as correlation density and the Spectral Fragility Index. These measures are computationally simple, can be updated at monthly frequency, and provide information about the current regional amplification state of the sovereign credit system. They should not be presented to policymakers as predictive instruments, but as nowcasting tools that sharpen the contemporaneous picture of regional stress.

Several extensions remain open. Future work could apply the framework to weekly or daily EMBI/CDS data, where the timing of stress propagation can be measured more precisely and where the contemporaneous-versus-predictive distinction can be tested at horizons short enough to make network amplification potentially leading rather than coincident. The approach could also be extended to other emerging-market regions to

assess whether finite-size sovereign avalanches are a Latin American phenomenon or a more general feature of emerging-market debt. A further extension would be to combine EMBI data with fund-flow, holdings, issuance, foreign-exchange, commodity-price, and macro-fiscal variables in order to move from descriptive contemporaneous association toward structural identification of the propagation mechanism, and to test whether richer multivariate predictive specifications can recover significant lead–lag content that the parsimonious bivariate analysis in this paper does not detect. Finally, the framework could be used for counterfactual policy simulations, evaluating whether shocks to specific sovereigns, global risk factors, or network links produce materially different regional avalanche distributions.

In sum, the paper does not claim that Latin American sovereign credit markets are governed by a pure self-organized critical law. It shows that they exhibit several of the empirical ingredients of finite-size criticality—heavy-tailed stress events, non-random synchronization, threshold-robust regional avalanches, and a contemporaneous network environment that becomes denser and more spectrally integrated during stress—while also showing that the network amplification signal is largely common-factor in nature and does not deliver robust early-warning content at the three-month horizon. For sovereign-risk surveillance, the implication is straightforward: regional fragility should be monitored not only through country fundamentals, but also through the dynamic geometry of sovereign credit co-movement, with appropriate attention to the distinction between contemporaneous regime descriptors and forward- looking predictive instruments.

References

- Acemoglu, D., Carvalho, V. M., Ozdaglar, A., and Tahbaz-Salehi, A. (2012). The network origins of aggregate fluctuations. *Econometrica*, 80(5):1977–2016.
- Acemoglu, D., Ozdaglar, A., and Tahbaz-Salehi, A. (2015). Systemic risk and stability in financial networks. *American Economic Review*, 105(2):564–608.
- Bak, P. (1996). *How Nature Works: The Science of Self-Organized Criticality*. Copernicus, New York.
- Bak, P., Chen, K., Scheinkman, J., and Woodford, M. (1993). Aggregate fluctuations from independent sectoral shocks: Self-organized criticality in a model of production and inventory dynamics. *Ricerche Economiche*, 47(1):3–30.
- Bak, P., Tang, C., and Wiesenfeld, K. (1987). Self-organized criticality: An explanation of the $1/f$ noise. *Physical Review Letters*, 59(4):381–384.

- Bak, P., Tang, C., and Wiesenfeld, K. (1988). Self-organized criticality. *Physical Review A*, 38(1):364–374.
- Bekaert, G., Ehrmann, M., Fratzscher, M., and Mehl, A. (2014a). The global crisis and equity market contagion. *Journal of Finance*, 69(6):2597–2649.
- Bekaert, G., Harvey, C. R., Lundblad, C. T., and Siegel, S. (2014b). Political risk spreads. *Journal of International Business Studies*, 45(4):471–493.
- Calvo, G. A. (1988). Servicing the public debt: The role of expectations. *American Economic Review*, 78(4):647–661.
- Clauset, A., Shalizi, C. R., and Newman, M. E. J. (2009). Power-law distributions in empirical data. *SIAM Review*, 51(4):661–703.
- Cole, H. L. and Kehoe, T. J. (2000). Self-fulfilling debt crises. *Review of Economic Studies*, 67(1):91–116.
- Diebold, F. X. and Yilmaz, K. (2014). On the network topology of variance decompositions: Measuring the connectedness of financial firms. *Journal of Econometrics*, 182(1):119–134.
- Edwards, S. (1984). Ldc foreign borrowing and default risk: An empirical investigation, 1976–80. *American Economic Review*, 74(4):726–734.
- Eichengreen, B. and Mody, A. (1998). What explains changing spreads on emerging-market debt: Fundamentals or market sentiment? *NBER Working Paper*, (6408).
- Forbes, K. J. and Rigobon, R. (2002). No contagion, only interdependence: Measuring stock market comovements. *Journal of Finance*, 57(5):2223–2261.
- Forman, R. (2003). Bochner’s method for cell complexes and combinatorial ricci curvature. *Discrete and Computational Geometry*, 29(3):323–374.
- Gabaix, X. (2009). Power laws in economics and finance. *Annual Review of Economics*, 1:255–294.
- Gabaix, X., Gopikrishnan, P., Plerou, V., and Stanley, H. E. (2003). A theory of power-law distributions in financial market fluctuations. *Nature*, 423(6937):267–270.
- Glasserman, P. and Young, H. P. (2016). Contagion in financial networks. *Journal of Economic Literature*, 54(3):779–831.
- Haldane, A. G. and May, R. M. (2011). Systemic risk in banking ecosystems. *Nature*, 469(7330):351–355.

- Hilscher, J. and Nosbusch, Y. (2010a). Determinants of sovereign risk: Macroeconomic fundamentals and the pricing of sovereign debt. *Review of Finance*, 14(2):235–262.
- Hilscher, J. and Nosbusch, Y. (2010b). Determinants of sovereign risk: Macroeconomic fundamentals and the pricing of sovereign debt. *Review of Finance*, 14(2):235–262.
- Kaminsky, G. L. and Reinhart, C. M. (2000). On crises, contagion, and confusion. *Journal of International Economics*, 51(1):145–168.
- Kaminsky, G. L., Reinhart, C. M., and Végh, C. A. (2003). The unholy trinity of financial contagion. *Journal of Economic Perspectives*, 17(4):51–74.
- Longstaff, F. A., Pan, J., Pedersen, L. H., and Singleton, K. J. (2011). How sovereign is sovereign credit risk? *American Economic Journal: Macroeconomics*, 3(2):75–103.
- Lux, T. and Marchesi, M. (1999). Scaling and criticality in a stochastic multi-agent model of a financial market. *Nature*, 397(6719):498–500.
- Mandelbrot, B. (1963). The variation of certain speculative prices. *Journal of Business*, 36(4):394–419.
- Mantegna, R. N. (1999). Hierarchical structure in financial markets. *The European Physical Journal B*, 11(1):193–197.
- Newman, M. E. J. (2005). Power laws, pareto distributions and zipf’s law. *Contemporary Physics*, 46(5):323–351.
- Ollivier, Y. (2009). Ricci curvature of markov chains on metric spaces. *Journal of Functional Analysis*, 256(3):810–864.
- Reinhart, C. M. and Rogoff, K. S. (2009). *This Time Is Different: Eight Centuries of Financial Folly*. Princeton University Press, Princeton, NJ.
- Reinhart, C. M. and Trebesch, C. (2016). Sovereign debt relief and its aftermath. *Journal of the European Economic Association*, 14(1):215–251.
- Sandhu, R., Georgiou, T., and Tannenbaum, A. (2016). Ricci curvature: An economic indicator for market fragility and systemic risk. *Science Advances*, 2(5):e1501495.
- Scheinkman, J. A. and Woodford, M. (1994a). Self-organized criticality and economic fluctuations. *American Economic Review*, 84(2):417–421.
- Scheinkman, J. A. and Woodford, M. (1994b). Self-organized criticality and economic fluctuations. *American Economic Review*, 84(2):417–421.

- Sornette, D. (2003). *Why Stock Markets Crash: Critical Events in Complex Financial Systems*. Princeton University Press, Princeton, NJ.
- Stumpf, M. P. H. and Porter, M. A. (2012). Critical truths about power laws. *Science*, 335(6069):665–666.
- Tumminello, M., Aste, T., Di Matteo, T., and Mantegna, R. N. (2005). A tool for filtering information in complex systems. *Proceedings of the National Academy of Sciences*, 102(30):10421–10426.
- Vallarino, D. (2026a). Identification and inference in nonlinear dynamic network models. *arXiv preprint*. arXiv:submit/7441433.
- Vallarino, D. (2026b). Sandpile economics: Theory, identification, and evidence. *arXiv preprint arXiv:2604.13890*.
- Vallarino, D. (2026c). Stochastic network survival dynamics: A nonlinear evolution problem on economic graphs. *Communications in Nonlinear Science and Numerical Simulation*, 159:109904.
- Vuong, Q. H. (1989). Likelihood ratio tests for model selection and non-nested hypotheses. *Econometrica*, 57(2):307–333.